Report of Investigation 2022-2

UPDATED TSUNAMI INUNDATION MAPS FOR KARLUK AND LARSEN BAY, KODIAK ISLAND, ALASKA

Elena N. Suleimani, J. Barrett Salisbury, and Dmitry J. Nicolsky

Larsen Bay Cannery. Photo: Department of Commerce, Community and Economic Development; Division of Community and Regional Affairs' Community Photo Library.

Published by
STATE OF ALASKA
DEPARTMENT OF NATURAL RESOURCES
DIVISION OF GEOLOGICAL & GEOPHYSICAL SURVEYS
2022

UPDATED TSUNAMI INUNDATION MAPS FOR KARLUK AND LARSEN BAY, KODIAK ISLAND, ALASKA

Elena N. Suleimani, J. Barrett Salisbury, and Dmitry J. Nicolsky

Report of Investigation 2022-2

State of Alaska
Department of Natural Resources
Division of Geological & Geophysical Surveys

STATE OF ALASKA
Mike Dunleavy, Governor

DEPARTMENT OF NATURAL RESOURCES
Akis Gialopsos, Acting Commissioner

DIVISION OF GEOLOGICAL & GEOPHYSICAL SURVEYS
David L. LePain, State Geologist and Director

Publications produced by the Division of Geological & Geophysical Surveys (DGGS) are available for free download from the DGGS website (dggs.alaska.gov). Publications on hard-copy or digital media can be examined or purchased in the Fairbanks office:

Alaska Division of Geological & Geophysical Surveys
3354 College Rd., Fairbanks, Alaska 99709-3707
Phone: (907) 451-5010 Fax (907) 451-5050
dggspubs@alaska.gov | dggs.alaska.gov

DGGS publications are also available at:
Alaska State Library,
Historical Collections & Talking Book Center
395 Whittier Street
Juneau, Alaska 99811

Alaska Resource Library and Information Services (ARLIS)
3150 C Street, Suite 100
Anchorage, Alaska 99503

Suggested citation:
Suleimani, E.N., Salisbury, J.B., and Nicolsky, D.J., 2022, Updated tsunami inundation maps for Karluk and Larsen Bay, Kodiak Island, Alaska: Alaska Division of Geological & Geophysical Surveys Report of Investigation 2022-2, 42 p., 2 sheets. https://doi.org/10.14509/30892

Contents

Figures

Tables

Appendix

Map Sheets

TSUNAMI INUNDATION MAPS FOR KARLUK AND LARSEN BAY, KODIAK ISLAND, ALASKA

Elena N. Suleimani[1], J. Barrett Salisbury[2], and Dmitry J. Nicolsky[1]

Abstract

We evaluate potential tsunami hazards for the Kodiak Island communities of Karluk and Larsen Bay, Alaska, by numerically modeling the extent of inundation from tsunami waves generated by hypothetical earthquakes. Credible worst-case scenarios are defined by analyzing the tsunami dynamics related to various plausible earthquake slip distributions along the Alaska–Aleutian megathrust. Potential worst-case tsunami sources include megathrust earthquakes in the Kodiak Island region with a magnitude range of M_W9.0 to M_W9.3. We do not include impacts of subaerial or submarine landslide tsunami sources, as that is beyond the scope of this study. A hypothetical earthquake near Kodiak Island with maximum slip distributed between 10 and 40 km depth (6.2–24.85 mi) results in "worst case" tsunami-inundation for both Karluk and Larsen Bay. The maximum predicted overland flow depth ranges from 5 to 10 m (17 to 33 ft) in Karluk and from 10 to 15 m (33 to 49 ft) in Larsen Bay. The currents can be as strong as 4 m/sec (7.8 knots) in Karluk River and 7 m/sec (13.6 knots) in Larsen Bay. Dangerous wave activity is expected to last for at least 12 hours after the hypothetical worst-case earthquakes. Tsunami inundation maps that accompany this report represent a combination of numerous tsunami scenarios to show the maximum composite extent of inundation from these models. Results presented here are intended to provide guidance to local emergency management agencies for tsunami inundation assessment, evacuation planning, and public education to mitigate future tsunami damage.

INTRODUCTION

In Alaska, subduction of the Pacific plate under the North American plate has resulted in numerous great (M > 8) earthquakes and is the source of locally generated tectonic tsunamis in Alaska (Dunbar and Weaver, 2008). Several 20th century tsunamis generated by Alaska–Aleutian subduction zone earthquakes have resulted in widespread damage and loss of life in exposed coastal communities throughout the Pacific (Lander, 1996). However, tsunamis originating in the vicinity of the Alaska Peninsula, Aleutian Islands, and the Gulf of Alaska are considered near-field hazards and could reach Alaska's coastal communities within minutes of an earthquake. Reducing property damage and loss of life is highly dependent on community preparedness.

On March 27, 1964, the largest earthquake ever recorded in North America struck Southcentral Alaska. This moment magnitude (M_W) 9.2 megathrust earthquake, known as the Great Alaska Earthquake (fig. 1), generated the most destructive tsunami in Alaska history and, farther south, impacted the west coast of Canada and the United States (Plafker and others, 1969; Kanamori, 1970;

[1]Alaska Earthquake Center, Geophysical Institute, University of Alaska, P.O. Box 757320, Fairbanks, Alaska 99775-7320; ensuleimani@alaska.edu
[2]Alaska Division of Geological & Geophysical Surveys, 3354 College Rd., Fairbanks, Alaska 99709-3707.

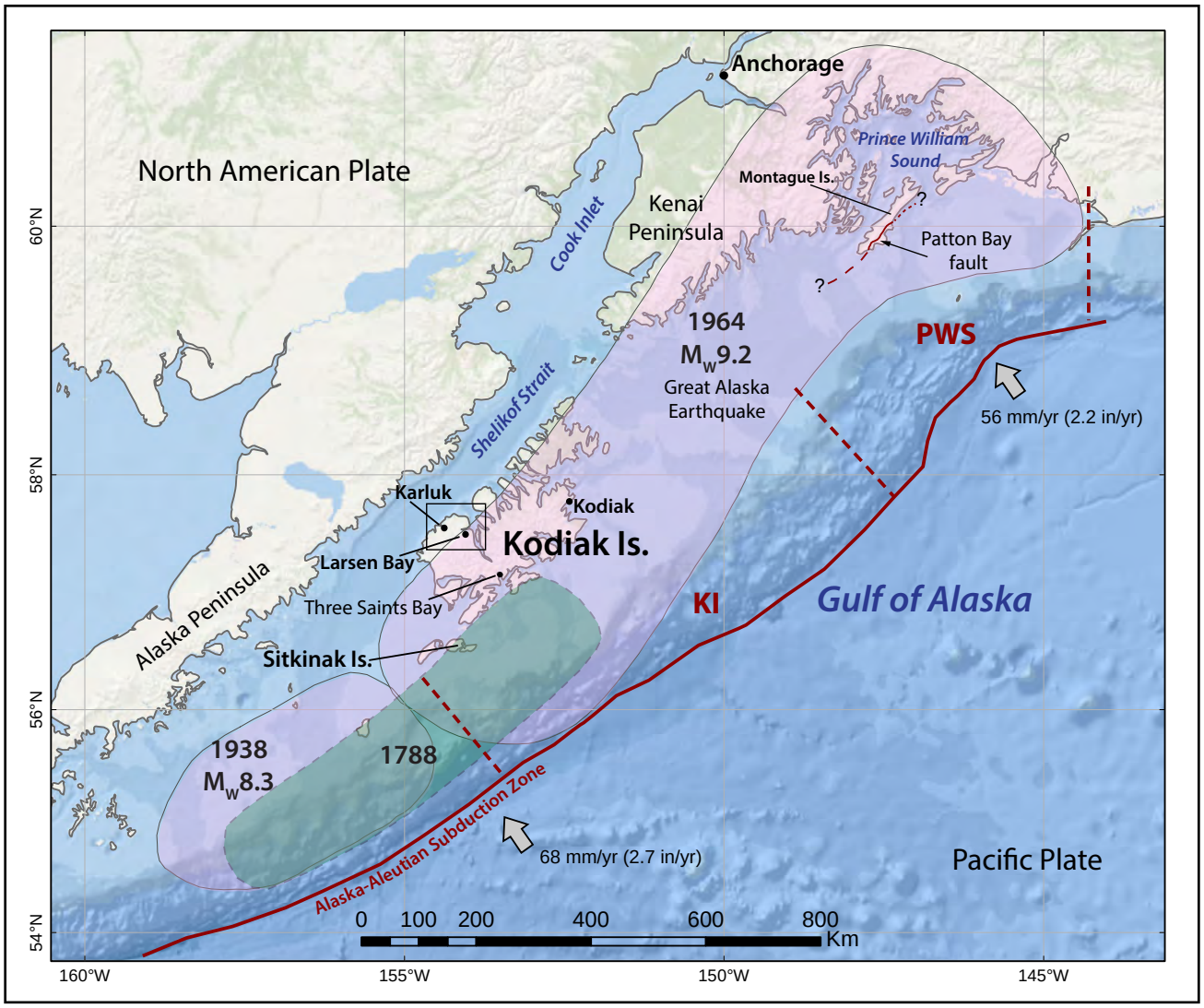

Figure 1. Map of Southcentral Alaska showing the location of Kodiak Island and the rupture zones of the 1788, 1938, and 1964 Alaska–Aleutian megathrust earthquakes (shaded areas). KI = Kodiak Island segment; PWS = Prince William Sound segment. The Patton Bay fault is shown by solid, dashed, and dotted lines where it is mapped with certainty, approximately, and inferred, respectively.

Johnson and others, 1996; Lander, 1996; Fine and others, 2018a; Fine and others, 2018b; Rabinovich and others, 2019). Kodiak, the largest community on Kodiak Island, suffered great losses from the earthquake and subsequent tsunami. Damage was primarily caused by 1.7 m (5.6 ft) of tectonic subsidence and a train of waves that inundated the low-elevation areas of town (Kachadoorian and Plafker, 1967). In addition to the major tectonic tsunami generated by an ocean-floor displacement in the Gulf of Alaska, numerous subaerial and submarine landslides generated local tsunamis in coastal communities (Lander, 1996). Landslide-generated tsunamis arrived almost immediately after the earthquake shaking and left no time for warning or evacuation. Of the 131 fatalities associated with this earthquake, 122 were caused by tsunami waves (Lander, 1996). Despite this relatively recent M_w 9.2 earthquake, the region still has high potential for future large earthquakes, and it is only a matter of time before another devastating tsunami—local or distant—strikes Alaska coastlines. Thus, estimating the potential flooding of the coastal zone is an essential component of the preparedness process.

The tsunami inundation maps for the Kodiak Island communities described in this report represent the results of the continuous combined effort of state and federal agencies to mitigate tsunami damage in coastal Alaska. The intended audience of this report consists of scientists, engineers, and planners interested in an applied approach to develop tsunami inundation and evacuation maps using a "worst-case scenario" modeling approach. Digital data and documentation provided with the report enable technical users to explore the range of possible tsunami inundation for future events. We use a deterministic approach for our earthquake and tsunami hazard modeling, which is distinctly different from the probabilistic tsunami hazard analysis used in projects with different objectives, such as land-use planning or insurance estimates (Geist and Parsons, 2006). We are less concerned about the probability that an earthquake of a certain magnitude will occur in a given amount of time and more focused on the tsunami inundation resulting from the largest hypothetical, yet scientifically defensible, earthquake scenarios that could potentially affect the communities. The methodologies used to develop tsunami inundation maps are described in detail in multiple publications and are not reviewed in this report. Refer to Suleimani and others (2016) for a complete description of the process.

PROJECT BACKGROUND: REGIONAL AND HISTORICAL CONTEXT

Setting

Kodiak Island is the largest island in Alaska and the second largest island in the United States (fig. 1). The following information is extracted from the Alaska Community Database maintained by the State of Alaska Division of Community and Regional Affairs of the Department of Commerce, Community, and Economic Development (DCCED/DCRA, 2015).

Kodiak island has been inhabited for the past 8,000 years. The first non-Native contacts were in 1763 by Russian Stephen Glotov and in 1792 by Alexander Baranov, a Russian fur trapper. Sea otter pelts were the primary incentive for Russian exploration, and a settlement was established at Chiniak Bay, the site of present-day Kodiak (fig. 1). At that time the island was called "Kikhtak," and later was known as "Kadiak," the Inuit word for island. In 1882 a fish cannery opened at the Karluk spit, sparking the development of commercial fishing in the area. Currently, there are several communities on Kodiak Island. Below we provide a short description of Karluk and Larsen Bay.

Karluk is located on the northwest coast of Kodiak Island, on the Karluk River, 88 air miles southwest of Kodiak City and 301 miles southwest of Anchorage (figs. 1 and 2). Karluk is an Alutiiq village with a fishing and subsistence lifestyle. The mouth of the Karluk River is thought to have been populated by Alaska Natives for more than 7,000 years. Thirty-six archaeological sites exist in the area. Russian hunters established a trading post here in 1786. At that time, the village was located on both sides of the Karluk River, near Karluk Lagoon. A post office was established in 1892. By 1900, Karluk was known for having the largest cannery and the greatest salmon stream in the world. In the early 1900s, canneries were constructed by the Alaska Packers Association. Over-fishing of the area forced the canneries to close in the late 1930s. After a severe storm in January 1978, the village council decided to relocate the community to the present site, upstream, on the south side of the lagoon.

Larsen Bay is located on Larsen Bay, on the northwest coast of Kodiak Island. It is 60 miles southwest of Kodiak City and 283 miles southwest of Anchorage (figs. 1 and 2). The area is thought to have been inhabited for at least 2,000 years. Hundreds of artifacts have been uncovered in the area. Russian fur traders frequented the island in the mid-1700s. The bay was named for Peter Larsen, an Unga Island furrier, hunter, and guide. The present-day Alaska Natives who reside in Larsen Bay are Alutiiq (Russian-Aleuts). The Alaska Packers Association built a cannery in the

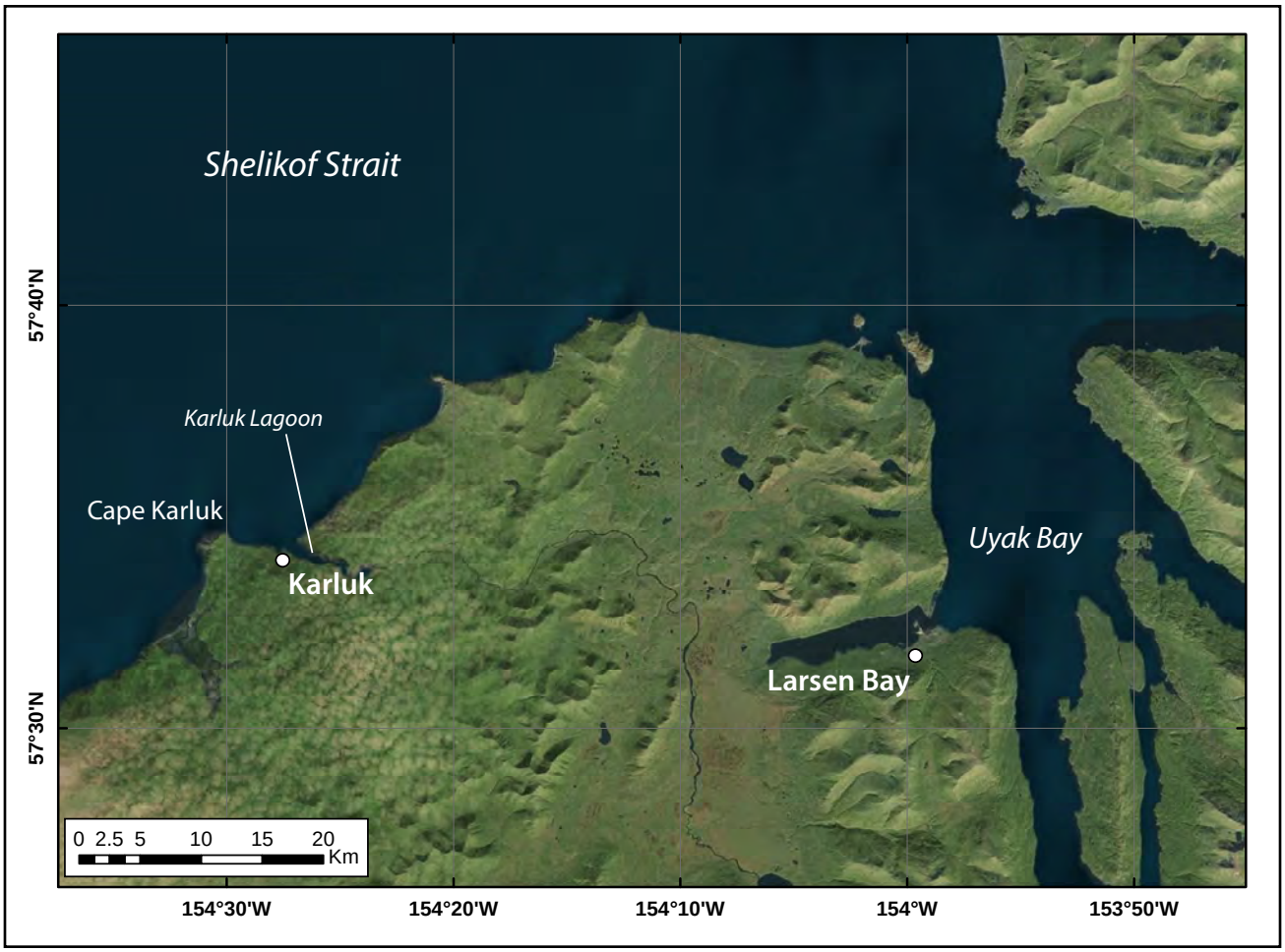

Figure 2. Satellite image showing locations of Karluk and Larsen Bay on the northwest shore of Kodiak Island.

village in 1911. The city was incorporated in 1974. The economy of Larsen Bay is primarily based on fishing. A large majority of the population depends on subsistence activities. Salmon, halibut, seal, sea lion, clams, crab, and deer are harvested. Six lodges host visitors and provide a tourist guide service.

SEISMIC AND TSUNAMI HISTORY

Kodiak Island is located at the eastern end of the Alaska–Aleutian subduction zone, the boundary along which the Pacific and North American tectonic plates converge (fig. 1). The rate of plate convergence near the island is approximately 60 mm (2.4 in) per year (DeMets and others, 1990), and the eastern end of the megathrust has produced significant tsunamigenic earthquakes. On March 27, 1964, Southcentral Alaska was struck by the M_W 9.2 Great Alaska Earthquake—the largest earthquake ever recorded in North America and the second largest ever recorded in the world after the 1960 magnitude M_W 9.5 off the coast of Chile. The Great Alaska Earthquake (fig. 1) generated a destructive tsunami that caused fatalities and great damage in Alaska, Hawaii, and the west coasts of the United States and Canada. The earthquake ruptured an 800-km-long (~500-mi-long) section of the Aleutian megathrust, producing vertical displacements over an area of about 285,000 km^2 (110,039 mi^2) in Southcentral Alaska (Plafker, 1969). The area of coseismic subsidence included Kodiak Island (KI), Kenai Peninsula, Cook Inlet, and part of northern Prince William Sound (PWS; fig. 1). The major zone of uplift was seaward of the subsidence zone, in the Gulf of Alaska (Plafker, 1969). Several communities on Kodiak Island suffered greatly from the resulting tsunami waves.

The penultimate tsunami event near Kodiak Island was recorded on July 21, 1788, when a strong earthquake near Sitkinak Island caused a 3–10 m (10–33 ft) tsunami that forced relocation of the first Russian settlement at Three Saints Bay on southwestern Kodiak Island (Soloviev, 1990; Lander, 1996) (fig. 1). Briggs and others (2014) present stratigraphic evidence of land level change and, together with ^{137}Cs and ^{210}Pb bracketing ages of a sand deposit that can be traced 1.5 km (0.93 mi) inland on Sitkinak Island (fig. 1), interpreted to be deposited by the tsunami, suggest that the 1788 earthquake was a large megathrust rupture that generated the tsunami.

Analysis of historical earthquake data in the PWS and KI regions (Nishenko and Jacob, 1990) showed that significant megathrust earthquakes occurred more frequently in the KI region and ruptured independently of the PWS region. For example, paleoseismic data show that the KI region ruptured independently in a large earthquake about 500 years ago—about 360 years more recently than the penultimate great earthquake that ruptured both the KI and PWS regions (Carver and Plafker, 2008). The PWS and KI regions have different recurrence intervals, with estimates of the recurrence interval for M 7.5–8 earthquakes in the KI segment being as low as 60 years (Nishenko, 1991).

Using seismic waveform data, Christensen and Beck (1994) showed that there were two areas of high "moment" (i.e., energy) release during the 1964 Great Alaska Earthquake. The two major asperities, or areas of maximum defined slip, form the overall 1964 rupture zone: the Prince William Sound asperity with an average slip of 18 m (59 ft), and the Kodiak Island asperity with an average slip of 10 m (33 ft) (fig. 1). The results of joint inversion of tsunami and geodetic data from the 1964 event (Johnson and others, 1996) also suggest two areas of high moment release. Subsequent studies have shown that the PWS asperity is on the Yakutat–North American megathrust, whereas the KI asperity is on the Pacific–North American megathrust (Ferris and others, 2003; Eberhart-Phillips and others, 2006; Worthington and others, 2010, 2012; Gulick and others, 2013).

The most recent deformation model of the 1964 earthquake by Suleimani and Freymueller (2020) incorporated updated fault geometries and the postseismic deformation that followed the earthquake (Suito and Freymueller, 2009), and observations of tsunami waves in the source area along the coast of the Kenai Peninsula and Kodiak Island.

This model used tsunami first arrivals on the Kenai Peninsula to constrain the extent of the Montague Island high-angle splay fault, the Patton Bay fault, from its subaerial outcrop to an extended length along the southern Kenai Peninsula (fig. 1). Suleimani and Freymueller (2020) showed that, along the south coast of Kodiak Island, coseismic slip on the megathrust alone is capable of producing tsunami arrivals and amplitudes that agree well with the observations, and that there is no evidence of the splay faults rupturing offshore Kodiak during the 1964 earthquake.

Based on published paleoseismic data for the region, Carver and Plafker (2008) calculate that the median intervals between the past eight great ($M > 8$) earthquakes in the PWS segment of the eastern Alaska–Aleutian subduction zone range from 333 to 875 years, with an average of 589 years. Shennan, Bruhn, and others (2014) analyzed new paleoseismic field data from three sites in the PWS segment and revised the recurrence intervals of great earthquakes in the PWS segment. Their results suggest that the intervals range from ~420 to ~610 years, with a mean of ~535 years, excluding the interval between the 1964 earthquake and the penultimate event, which is ~883 years.

Recently, Shennan, Bruhn, and others (2014) presented paleoseismic data from Kodiak Island suggesting the intervals between ruptures of the KI segment are shorter than previously assumed, and that the KI segment ruptures more frequently than the PWS segment. The authors combined the analysis of new paleoseismic and radiocarbon data with previous historical and archaeological investigations

to show that the KI single-segment ruptures of 1788 and of ca. A.D. 1440–1620 both occurred between the multi-segment ruptures of the 1964 earthquake and the earthquake of ca. A.D. 1020–1150, when the PWS and KI segments ruptured together (Carver and Plafker, 2008; Shennan, Bruhn, and others, 2014). Shennan, Barlow, and others (2014) also analyzed the patterns of uplift and subsidence for the three most recent events on the KI segment—the 1964, the 1788, and the ca. A.D. 1440–1620 earthquakes—and found that the location of the hinge line, or the contour of zero vertical deformation (between regions of uplift and subsidence), was different for all three events.

Briggs and others (2014) presented stratigraphic evidence of land-level change and tsunami inundation during prehistoric and historical earthquakes west of Kodiak Island. They reported mixed uplift and subsidence records for Sitkinak Island (fig. 1), which suggests that it is located above a nonpersistent boundary near the edge of the 1964 rupture. This island experienced either uplift or subsidence, depending on where the ruptures stopped along strike.

Karluk and Larsen Bay have been impacted by tsunamis in the past, as documented by the National Centers for Environmental Information/World Data Centers (NCEI/WDS) Global Historical Tsunami Database (in progress) and Lander (1996). Table 1 summarizes the effects of the 1964 tsunami that were experienced by Karluk and Larsen Bay.

Landslide-Generated Tsunami Hazards

Tsunamis caused by submarine and subaerial slope failures are a significant hazard in the fjords of coastal Alaska and other high-latitude fjord coastlines (Lee and others, 2006). Kulikov and others (1998) analyzed tsunami catalog data for the northern Pacific coast and showed that this region has a long record of tsunami waves generated by submarine and subaerial landslides, avalanches, and rockfalls. For example, numerous local submarine and subaerial landslide tsunamis were generated in 1964, causing 76 percent of the tsunami fatalities associated with the Great Alaska Earthquake (Lander, 1996). Long-duration ground shaking of the 1964 event triggered numerous rockslides, rockfalls, rotational slumps, and debris avalanches on the slopes of Kodiak Island.

Plafker and Kachadoorian (1966) documented and classified the observed landslides and provided a map of the distribution of the larger

Table 1. Tsunami effects at Karluk and Larsen Bay; data from the National Centers for Environmental Information/World Data Centers (NCEI/WDS) Global Historical Tsunami Database (in progress) and quoted comments from Lander (1996).

Date	Magnitude (MW)	Origin	Maximum water height ft (m)	Comments
Karluk				
03/27/1964	9.2	Gulf of Alaska	?	Karluk experienced the tsunami as low tide changes beginning 1.5 hours after the earthquake. It did not cause any damage.
Larsen Bay				
03/27/1964	9.2	Gulf of Alaska	4 (1.22)	Larsen Bay subsided 2.5 feet. A wave 4 feet over the high tide level at 1:00 A.M. caused two feet of water in the Alaska Packers Association warehouse. There was little significant damage. Rancher Dewitt Fields reported he lost a few head of cattle and some small buildings. Max amplitude 1.2 m. Warehouse flooded, sheds destroyed, and cattle drowned.

landslides and slope failures on Kodiak Island. In 1964, most ground failures were located along the southeastern shore of Kodiak Island. The concentration of slides along the southeast coast and the scarcity of them elsewhere appeared to be controlled by local rock type, as slope steepness was not found to be an important factor that controlled the distribution of slope failures around the island (Plafker and Kachadoorian, 1966). The authors showed a strong correlation between the maximum concentration of slides and outcrops of bedded Tertiary rock, the physical properties of which likely contributed to slide initiation. The map of ground shaking intensity suggests that ground accelerations in areas underlain by Tertiary rock were greater than in areas underlain by pre-Tertiary rock (Plafker and Kachadoorian, 1966). Another factor that probably contributed to the slide concentration along the southeastern shore was that large aftershocks were also located closer to that shore, and therefore caused a higher intensity of ground motion.

There were no observations or documented evidence of subaerial landslides reaching the water and generating waves during the 1964 earthquake. Even though subaerial and submarine landslides may occur in the next significant earthquake, there are insufficient data to appropriately constrain landslide tsunami sources. Therefore, in this report we do not model tsunamis generated by landslides.

METHODOLOGY AND DATA

Grid Development and Data Sources

We use a series of nested computational grids in the Kodiak Island area to generate detailed maps of potential tsunami inundation triggered by local and distant earthquakes. The coarsest grid, with 2-arc-minute (approximately 2 km [~1.2 mi]) resolution, spans the central and northern Pacific Ocean. We used three intermediate grids between the coarsest- and highest-resolution grids (table 2; fig. 3). The highest-resolution level 4 grids (shaded rectangles in fig. 3) cover Karluk and Larsen Bay. The spatial resolution of the high-resolution grids, with about 15 × 16 m (49.2 × 52.5 ft) cell dimensions, satisfies National Oceanic and Atmospheric Administration (NOAA) minimum recommended requirements for computation of tsunami inundation (National Tsunami Hazard Mapping Program [NTHMP], 2010).

Table 2. Nested grids used to compute propagation of tsunami waves generated in the Pacific Ocean to the Kodiak Island communities. The high-resolution grid is used to compute the inundation. Note that the grid resolution in meters is not uniform: the first dimension is the longitudinal grid resolution and the second is the latitudinal resolution.

Grid name	Resolution		West–East boundaries	South–North boundaries
	arc-seconds	feet (meters)		
Level 0, Northern Pacific	120 × 120	≈6,611 x 12,139 (2,015 × 3,700)	120°00'00" E–100°00'00" W	10°00'00" N–65°00'00" N
Level 1, South-central Alaska	24 × 24	≈ 1,322 x 2,428 (403 × 740)	156°00'00" W–145°00'00" W	55°00'00" N–62°00'00" N
Level 2, Coarse resolution, Kodiak Island	8 × 8	≈ 443 x 810 (135 × 247)	155°38'36" W–149°50'33" W	56°01'45" N–59°02'06" N
Level 3, Fine resolution, Kodiak Island	8/3 × 8/3	≈ 148 x 269 (45 × 82)	153°38'48" W–151°51'31" W	57°32'22" N–58°04'09" N
Level 4, High resolution, Karluk	8/9 × 1/2	≈ 49 × 52 (15 × 16)	154°33'18" W–154°22'21" W	57°32'58" N–57°36'29" N
Level 4, High resolution, Larsen Bay	8/9 × 1/2	≈ 49 × 52 (15 × 16)	154°8'4" W–153°54'19" W	57°31'14"N–57°34'54" N

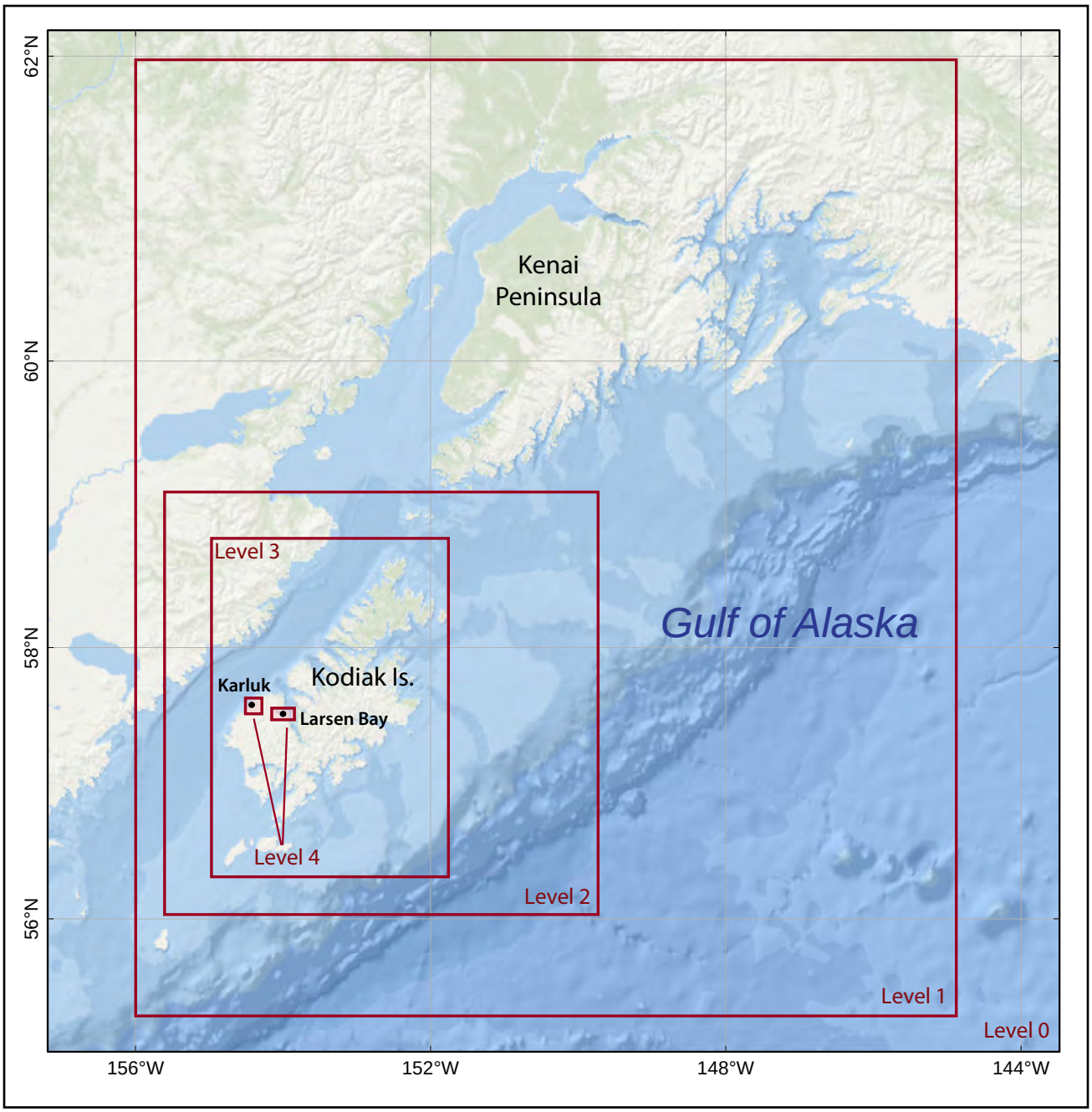

Figure 3. Nesting of the levels 0–4 bathymetry/topography grids for numerical modeling of tsunami propagation and runup in the Kodiak Island area. Each embedded grid is outlined by a red rectangle.

To develop the high-resolution level 4 grid, digital bathymetric, topographic, and shoreline datasets were obtained from various agencies, as described in Carignan and others (2013). The bathymetric datasets include National Ocean Service (NOS) hydrographic surveys, NOAA Electronic Navigational Chart (ENC) soundings, a U.S. Army Corps of Engineers (USACE) harbor survey, and multi-beam swath sonar surveys. The topographic datasets include the city of Kodiak bare-earth lidar digital elevation model (DEM) and the IFSAR DEM, the USGS National Elevation Dataset (NED) topographic DEM, and the USACE topographic points. More detailed information on grid development is contained in Lim and others (2009) and Carignan and others (2013).

Numerical Model of Tsunami Propagation and Runup

To estimate tsunami propagation and runup in the Kodiak area we used the same numerical modeling techniques as other Alaska tsunami inundation studies (for example, Suleimani and others, 2010, 2013, 2015, 2016, Nicolsky and others, 2013, 2014, 2015, and Nicolsky, Suleimani, Combellick, and Hansen, 2011). All hypothetical tsunami simulations were conducted using the bathymetric/topographic data corresponding to the Mean Higher High Water (MHHW) tide level in the Kodiak Island communities. Because the numerical model of tsunami propagation and runup does not dynamically simulate interaction of tides and tsunami waves, we use a conservative approach and assume that all simulated tsunamis arrive during high tides. To test the accuracy of the grid nesting around the Kodiak Island communities and verify our approach, we modeled the Tohoku tsunami of March 11, 2011, which is described in detail in Suleimani and others (2017).

The numerical modeling results presented in this report are relevant for existing sea level conditions and do not consider ongoing changes in water levels caused by global sea level rise, regional tectonic processes, and isostatic rebound. Even though the report on global sea level changes for 2050 and 2100 by the Intergovernmental Panel on Climate Change (Oppenheimer and others, 2019) predicts global sea level rise, the rapid regional uplift in southern Alaska caused by ice loss contributes to negative sea level changes in the region (Larsen and others, 2004; Shirzaei and others, 2021).

TSUNAMI SOURCES

It is generally thought that all the great historic earthquakes along the Alaska–Aleutian subduction zone occurred on the megathrust—the fault, or contact surface, between the subducting Pacific plate and the overriding North American plate. Friction between the two converging plates generally keeps them stuck, or "locked" together at the edges, but as the rest of the tectonic plates continue to move, shear stresses cause a build-up of elastic strain energy. The shear strain eventually overcomes the friction and strength of the rocks, and the energy is released during an earthquake, propagating through the ground and causing strong shaking associated with earthquakes. It is theorized that the shear strain primarily accumulates in the locked, or coupled regions of the megathrust where the friction on the fault is greatest.

Zweck and others (2002) used a three-dimensional elastic dislocation model to demonstrate that the GPS data in southern Alaska can be satisfied by the presence of a locked area near southwest Prince William Sound and a locked area near southwest Kodiak Island. They found that these locked areas correspond to the Prince William Sound and Kodiak Island asperities that ruptured in 1964, and that the locked regions repeat from one earthquake cycle to another. The authors showed that the site velocities on Kodiak Island are consistent with a model of plate locking near Kodiak Island, and that elastic strain is accumulating in the area.

Recent paleoseismological findings indicate that prehistoric and historical earthquakes that occurred on the KI segment of the Alaska–Aleutian megathrust have different spatial patterns of coseismic deformation, in both the along-strike and downdip directions (Briggs and others, 2014; Shennan, Barlow, others, 2014). The varying patterns of coseismic deformation mean that earthquakes, while all occurring within the KI segment, may rupture different lateral extents and result in energy release at different depths of the plate interface. The role of downgoing plate topography in fault segmentation and strain release is debated, with high relief topography thought to potentially be both barriers to and triggers for rupture. Increases in mechanical coupling may strengthen the plate boundary, but changes in fault zone physical properties (e.g., fracturing and fluid content) may limit strain accumulation. The geologic history and recent seismic imaging of the Alaska–Aleutian subduction zone suggest that the interface is complex and warrants further study, as it

may exert controls on rupture behavior. Because the width of the plate interface around Kodiak Island is quite large (measured in the down-dip direction, see fig. 4), earthquakes in this area do not necessarily rupture the whole interface every time. Therefore, our goal is to determine the segments of the interface that are most likely to rupture in the next large or great earthquake and model the tsunami dynamics associated with each hypothetical scenario.

The part of the plate interface extending from the seafloor trench to depths of 30–40 km (19–25 mi) is locked and accumulating strain. The dip of the subducting plate increases (steepens) from a 10° dip near the seafloor trench to a 30–45° dip at 30–40-km (19–25 mi) depth, which also corresponds to the boundary between the locked and transition zones (Carver and others, 2008). Locating the updip limit of the locked zone near Kodiak Island is hindered by the lack of geodetic data close to the Aleutian trench, and this zone is essentially unconstrained by the land-based geodetic data. Because we do not yet have seafloor GPS/acoustic measurements that are necessary to determine the behavior of the uppermost portion of the plate interface, we performed some additional steps to construct maximum credible earthquake and tsunami scenarios for Karluk and Larsen Bay. Recent studies comparing the Alaska and Tohoku tectonic margins (Kirby and others, 2013) suggest that there are several key geologic similarities between the two areas, and that

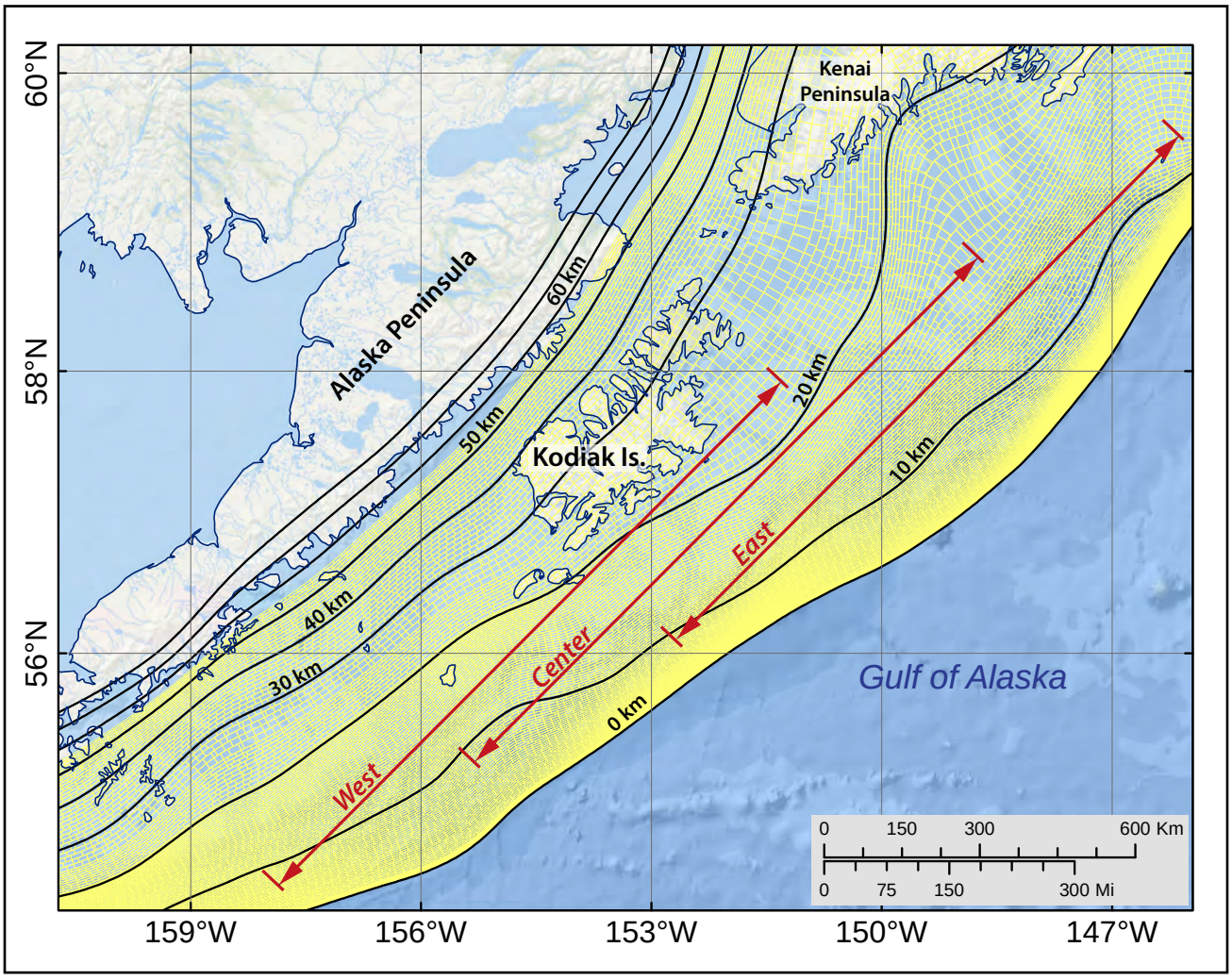

Figure 4. Discretization of the plate interface used to compute the coseismic vertical displacements with formulae developed by Okada (1985). Black lines mark depth contours (in kilometers) of the plate interface. Red arrows indicate along-strike extents of the three regions on which the sensitivity tsunami scenarios are based.

a hypothetical rupture might propagate to shallow depths on the Alaska–Aleutian megathrust, similar to what occurred during the M_W 9.0 Tohoku earthquake. Therefore, in our scenarios, we include earthquakes that rupture the shallow locked zone. Additionally, we conduct a sensitivity study to determine what effect the down-dip location of a rupture has on tectonic subsidence and uplift and resulting tsunami waves. The results of the sensitivity study are then used to construct earthquakes that generate maximum potential tsunami scenarios.

Sensitivity Study

Earthquake ruptures with slip at different depths result in different distributions and amounts of subsidence and uplift in coastal communities, and therefore in different tsunami and permanent flooding characteristics. The point of the sensitivity study is to determine the most dangerous location on the megathrust for a hypothetical earthquake to generate impactful tsunamis. To accomplish this, we generate a standardized set of M_W 9.0 earthquake ruptures and selectively place them at different along-strike and down-dip locations on the megathrust interface to determine which maximum slip locations will produce the worst-case combination of tectonic subsidence and tsunami inundation (detailed in this section). Later, we use these insights to develop the hypothetical earthquake scenarios (described in the next section and shown in table 3) to calculate inundation in specific communities.

We use the U.S. Geological Survey (USGS) SLAB2 model of the Alaska–Aleutian plate interface developed by Hayes (2018). Like the plate reconstruction by Zweck and others (2002), the SLAB2 plate interface model exhibits a relatively shallow dip angle beneath Kodiak Island and the Kenai Peninsula until it reaches a depth of 50 km (31 mi), at which point it steepens. The deep, steep area also corresponds to the unlocked (weakly coupled) part of the plate interface (fig. 4).

The plate interface is discretized into a mesh of rectangles ranging from 1 to 6 km (0.6 to 3.7 mi; yellow rectangles; fig. 4) in the along-strike direction. The upper and lower edges of each rectangle coincide with 0.5 km (0.3 mi) depth contours except in the shallowest part of the plate interface. Denser discretization for the top 5 km (3.1 mi) of the plate interface uses 0.25 km (0.16 mi) depth contours. The rectangles, called subfaults, are used to compute coseismic ground deformation (Okada, 1985) by first prescribing a general slip distribution for the proposed rupture, and then computing the slip at the center of each subfault using total seismic moment (energy release) as a constraint. The Kodiak Island area of the Alaska–Aleutian megathrust is one of the two large segments of the 1964 rupture zone with a very wide locked region (200–250 km [124.3–155.3 mi] wide in the downdip direction), but the detailed shape of the locked region is uncertain (Freymueller and others, 2008).

First, we divide the area around Kodiak Island into three along-strike regions: the "west," "center," and "east" segments (fig. 4). Karluk and Larsen Bay are located on the north-western shore of the island (fig. 1); therefore, a tsunami could reach them from both the northeast and the southwest. Placing potential tsunamigenic earthquake ruptures in these three segments allows us to cover all possible wave paths to the communities. For each segment we develop slip cases at four different depths (cases A–D) for a M_W 9.0 earthquake in the partially locked megathrust near Kodiak Island (Freymueller and others, 2008). These 12 sensitivity scenarios cover all sections of the megathrust in the KI segment, both in along-strike and down-dip directions. The slip distribution for all cases is uniform in the along-strike direction with tapering at the ends of the rupture (fig. 5). The assumed slip distribution is consistent with earthquake source scenarios used by other tsunami modeling studies (for example, Butler, 2014; USGS SAFRR scenario, www2.usgs.gov/natural_hazards/safrr/projects/tsunamiscenario.asp [SAFRR Tsunami Modeling Working Group, 2013]). Between any two consecutive cases, the hypothetical rupture is offset by about 10 km (6.2 mi) in the downdip direction: case A corresponds to a shallow surface-breaching

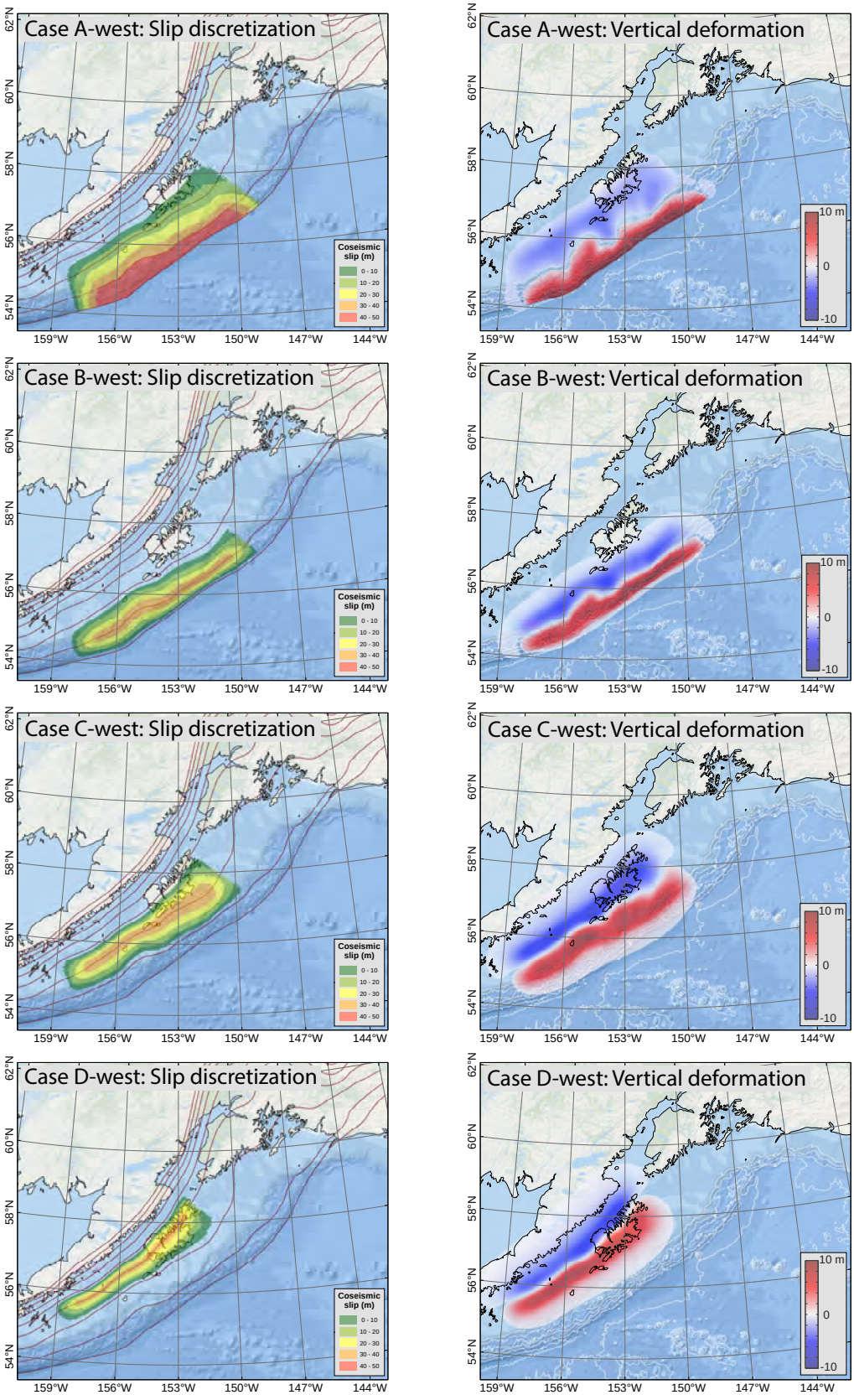

Figure 5A. Slip distribution along the plate interface (left), and computed vertical ground-surface deformation (right) for M_w 9.0 ruptures near Kodiak Island (sensitivity study cases A–D; west, center, and east). The slip location varies in the downdip direction of the plate interface while preserving the same patch configuration. Red lines are depth contours of the subduction interface, in kilometers. White lines are bathymetry contours within the depth interval between 1 and 5 km.

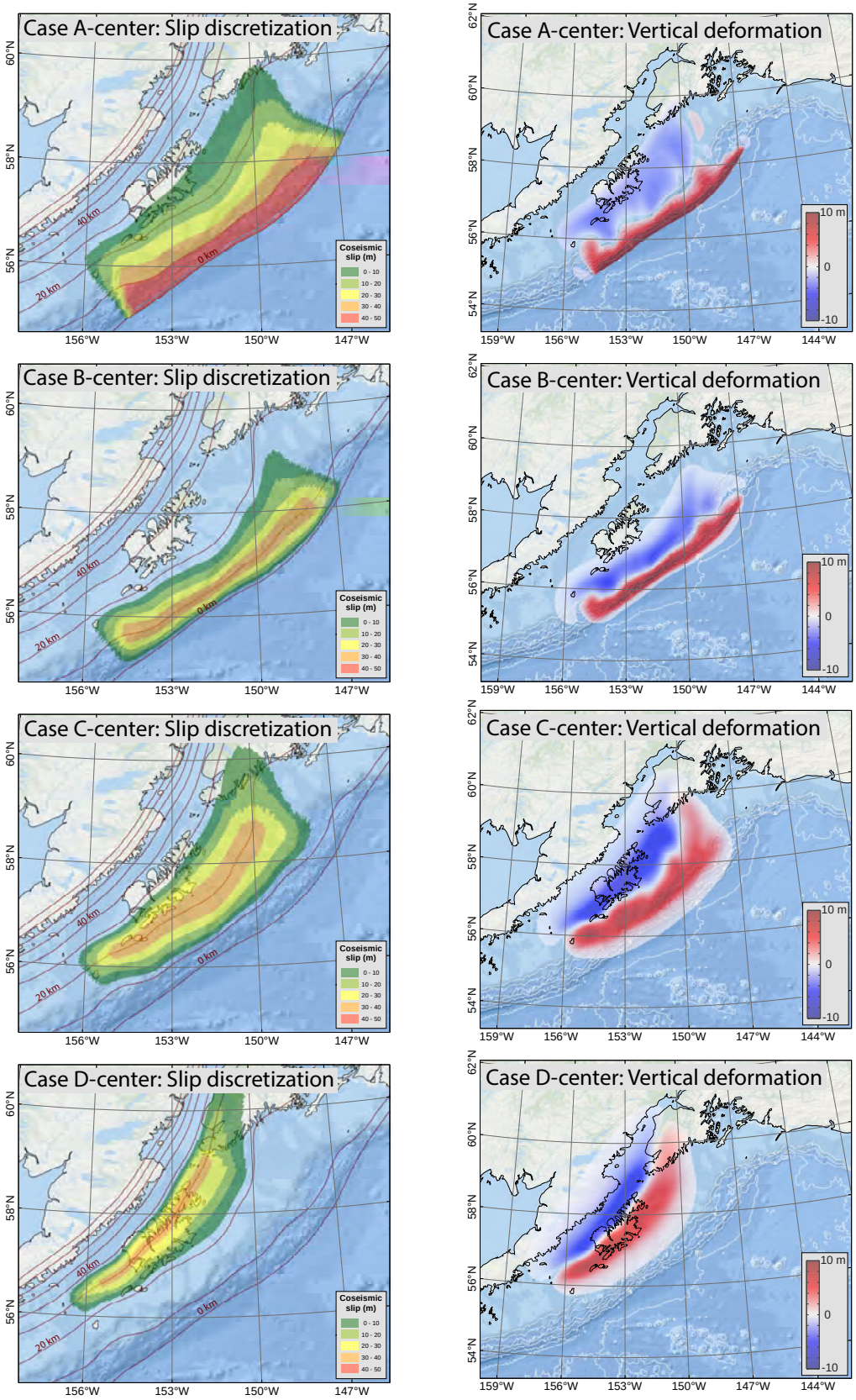

Figure 5B. Slip distribution along the plate interface (left), and computed vertical ground-surface deformation (right) for M_w 9.0 ruptures near Kodiak Island (sensitivity study cases A–D; west, center, and east). The slip location varies in the downdip direction of the plate interface while preserving the same patch configuration. Red lines are depth contours of the subduction interface, in kilometers. White lines are bathymetry contours within the depth interval between 1 and 5 km.

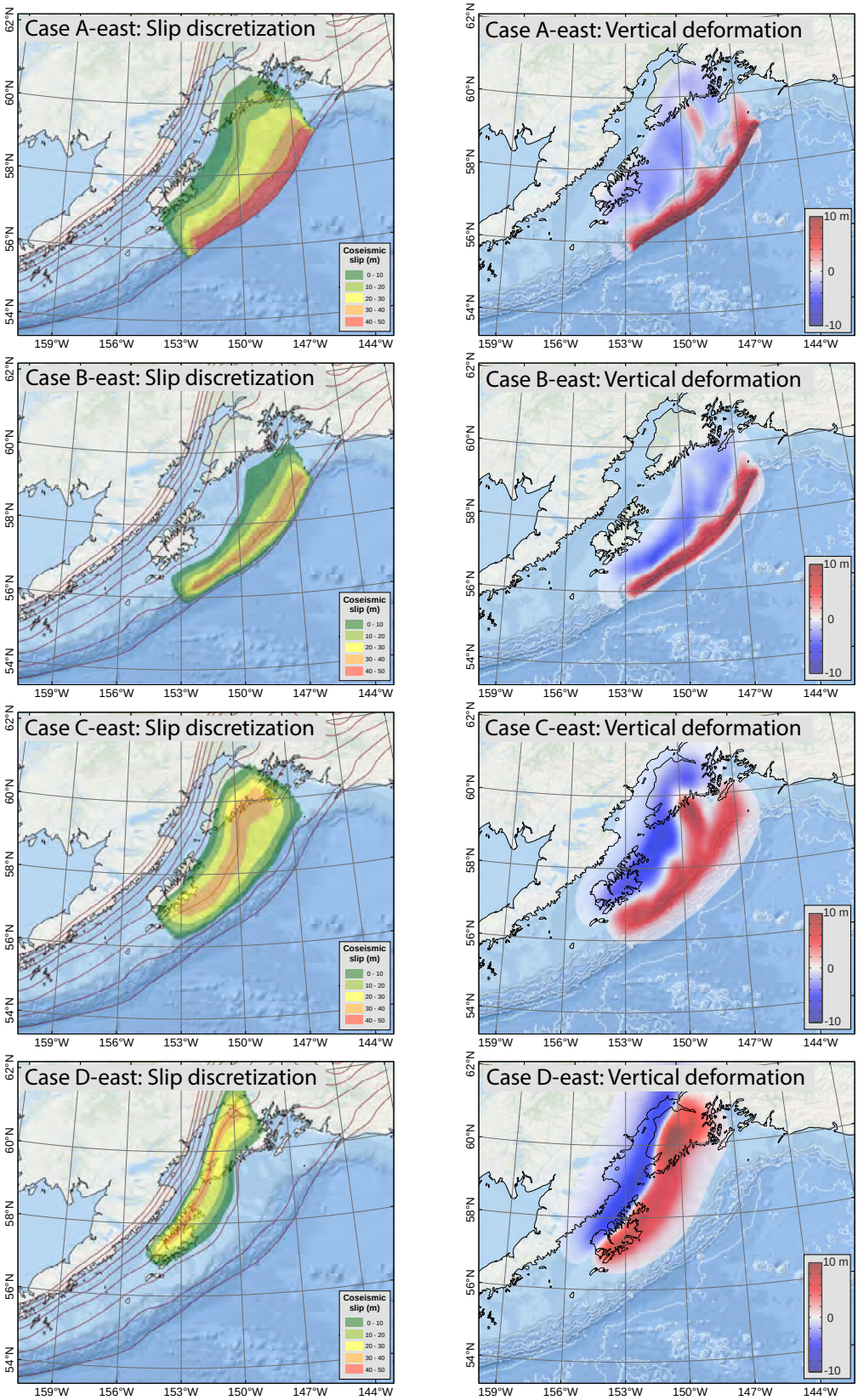

Figure 5C. Slip distribution along the plate interface (left), and computed vertical ground-surface deformation (right) for M_w 9.0 ruptures near Kodiak Island (sensitivity study cases A–D; west, center, and east). The slip location varies in the downdip direction of the plate interface while preserving the same patch configuration. Red lines are depth contours of the subduction interface, in kilometers. White lines are bathymetry contours within the depth interval between 1 and 5 km.

rupture with maximum amount of slip located close to the trench; case B corresponds to a rupture at 10 km (6.2 mi) depth; case C corresponds to a rupture at 20 km (12.4 mi) depth; and case D corresponds to a rupture at 30 km (18.6 mi) depth. We calculate vertical ground surface deformations associated with each case as an input for the tsunami model (fig. 5).

Community-specific tsunami wave dynamics at Karluk and Larsen Bay vary considerably according to different slip distributions (figs. 6 and 7). A rupture at a depth of 30 km (18.6 mi) (case D), which corresponds to the greatest coseismic subsidence in the communities, results in the highest wave amplitude at both locations. A rupture at a depth of 20 km (12.4 mi) (case C) also results in coseismic subsidence in both communities, resulting in the second-highest tsunami amplitudes. In Larsen Bay, case C results in an earlier wave arrival than case D. We also analyze the extent of inundation at Karluk and Larsen Bay for all sensitivity scenarios. For each community, we plot the inundation lines corresponding to the three worst-case sensitivity scenarios in figures 8 and 9 for Karluk and Larsen Bay, respectively. All worst-case inundation lines correspond to case D in both communities. One scenario, the case C rupture in the western segment, also produces sizable inundation in Larsen Bay.

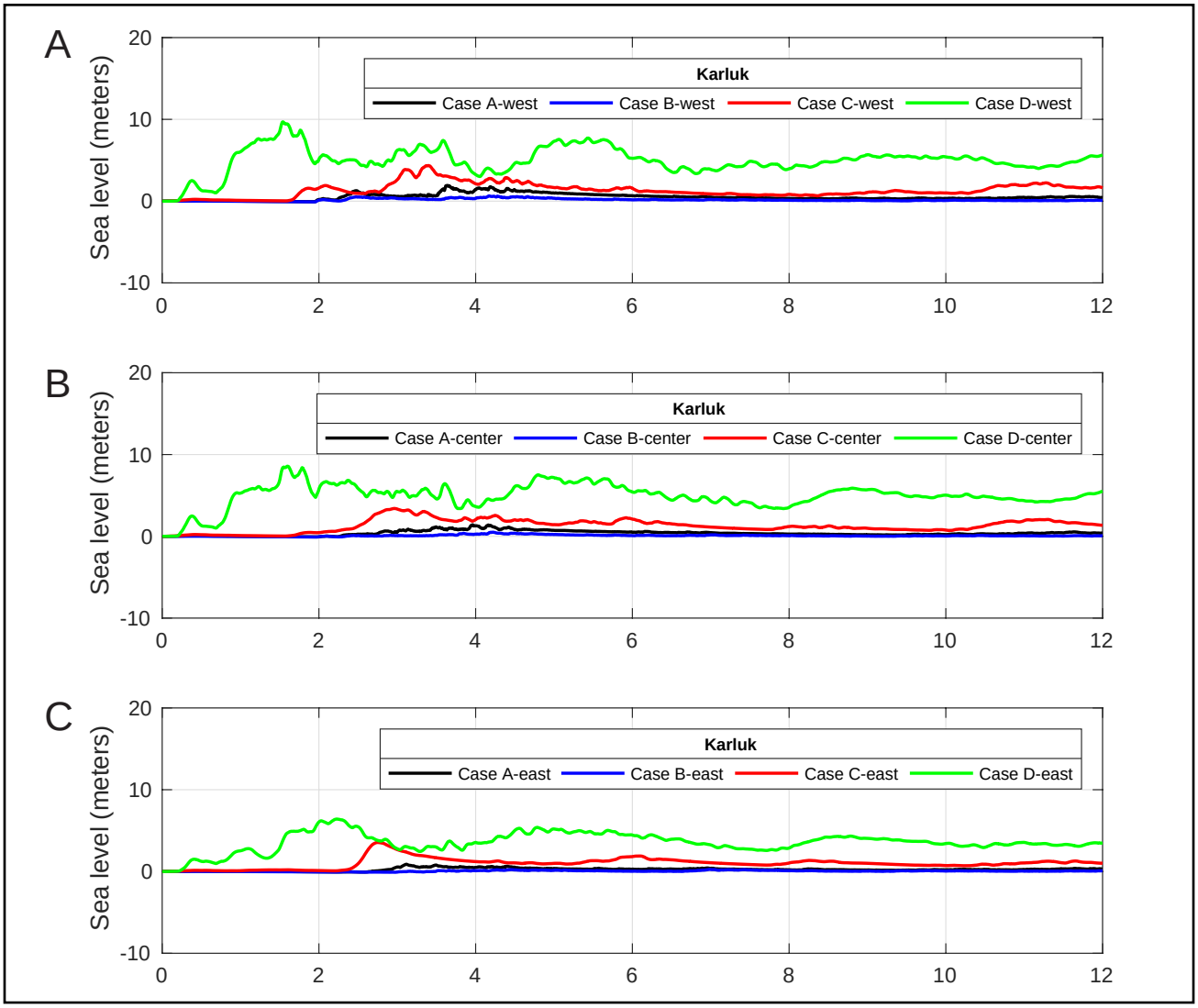

Figure 6. Modeled water-level dynamics (from the point of view of an observer standing at the shore) at Karluk for the ground-surface deformations shown in figure 5.

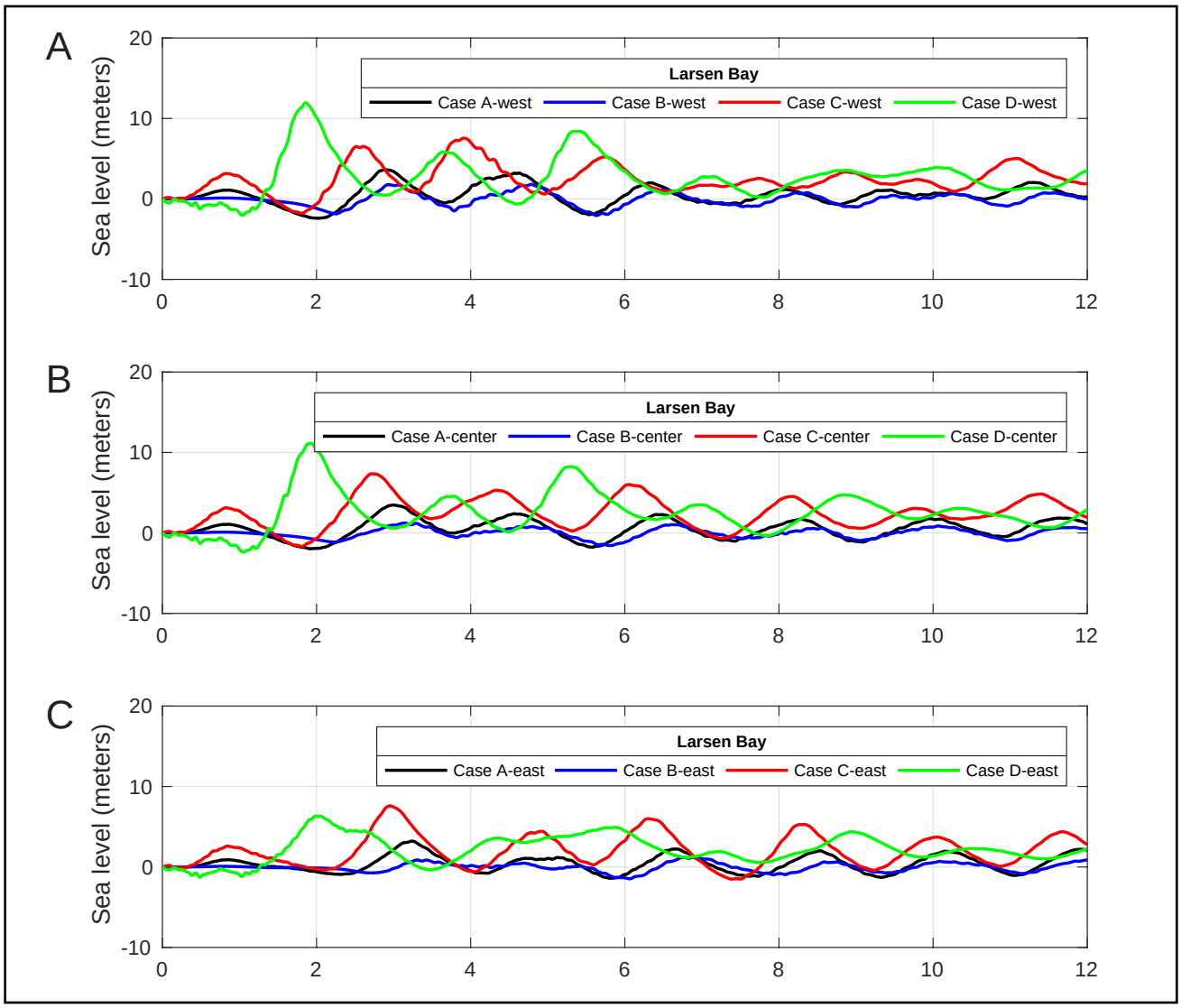

Figure 7. Modeled water-level dynamics (from the point of view of an observer standing at the shore) at Larsen Bay for the ground-surface deformations shown in figure 5.

Based on these results, we develop hypothetical ruptures with maximum slip in the 20–30 km (12.4–18.6 mi) depth range (cases C and D). As in Nicolsky and others (2016), we developed maximum credible scenarios for the Kodiak Island communities by assuming a slip up to 35 m (115 ft) in the deep and intermediate sections of the Alaska–Aleutian megathrust and up to 50 m (164 ft) in the shallow sections of the megathrust. The maximum slip is imposed along regions of the megathrust that have the capability to generate the highest amplitude waves coupled with the greatest amount of tectonic subsidence near Kodiak Island communities.

Hypothetical Tsunami Sources

In this section, we list Alaska–Aleutian megathrust earthquake scenarios near Kodiak Island (table 3). Our goal is to determine geologically plausible scenarios that will result in maximum tsunami inundation in Kodiak Island communities—"credible worst-case scenarios." They are based on results of the sensitivity study (scenarios 1–5), geodetic data, and new thoughts regarding local megathrust behavior (scenarios 6–8). Previously, the coseismic slip was limited to 18.5 m (60.7 ft) near the trench (figure 6 in Suleimani and others, 2005). Now, following modeling results for the

Figure 8. Extents of tsunami inundation at Karluk for selected sensitivity scenarios.

USGS SAFRR project and considering implications of the 2011 Tohoku earthquake (Wang and others, 2018), we suggest that the maximum slip near the trench could be up to 50 m (164 ft). Also, for the sake of consistency with previous reports (e.g., Nicolsky and others, 2016, 2017; Suleimani and others, 2016), we consider two earthquakes (scenarios 7 and 8) with slip parameterization according to research by Butler and others (2014).

In all scenarios, we do not account for the finite speed of rupture propagation along the fault and we consider the ocean-bottom displacements to be instantaneous. All examined scenarios are summarized in table 3. The proposed slip distributions and vertical coseismic deformations are shown in figure 10.

In scenarios 1–5, we assume a maximum slip at depths of 20 and 30 km (12.4 and 18.6 mi)—the most sensitive depths for Kodiak Island communities. In the downdip direction, the slip is determined by the slip skewness parameter q in the Freund and Barnett (1976) formulae, and the along-strike slip distribution is uniform. For each scenario, the maximum slip is assumed to be located at a different depth range. In scenarios 6–8, we account for the earthquake deformation front reaching the seafloor by extending the fault slip all the way to the zero-depth contour. Scenario 9 models a rupture of the Cascadia subduction zone as an example of a distant tsunami source. We note that the presented scenarios intend to capture the maximum credible scenarios and provide a starting point for development of more complex models.

Figure 9. Extents of tsunami inundation at Larsen Bay for selected sensitivity scenarios.

Table 3. Hypothetical megathrust scenarios used to model tsunami runup in Karluk and Larsen Bay. Asterisk indicates scenarios that have been considered in previous inundation mapping reports and "q" is the slip skewness parameter of Freund and Barnett (1976).

Scenario number	Description	Depth range, km (mi)	Maximum slip depth range, km (mi)	Maximum slip, m (ft)	Maximum subsidence, m (ft)	Maximum uplift, m (ft)
1	M_w 9.2 earthquake near Kodiak Island; 20 km depth	10-30 (6.2-18.6)	15-25 (9.3-15.5)	35.0 (115.0)	6.9 (22.6)	9.4 (30.8)
2	M_w 9.0 earthquake near Kodiak Island; 30 km depth	20-40 (12.4-24.8)	25-35 (15.5-21.7)	35.0 (115.0)	6.4 (21.0)	8.7 (28.5)
3	M_w 9.3 earthquake near Kodiak Island; 20-30 km depth	10-40 (6.2-24.8)	15-35 (9.3-21.7)	35.0 (115.0)	7.9 (25.9)	10.5 (34.4)
4	M_w 9.27 earthquake near Kodiak Island; 20-30 km depth, q=0.2	10-40 (6.2-24.8)	12-22 (6.5-13.7)	35.0 (115.0)	5.0 (16.4)	11.4 (37.4)
5	M_w 9.18 earthquake near Kodiak Island; 20-30 km depth, q=0.7	10-40 (6.2-24.8)	15–25 (9.3-15.5)	35.0 (115.0)	7.3 (23.9)	7.7 (25.2)
6	M_w 9.3 earthquake near Kodiak Island; 10 km depth, slip extending to 0 km depth	0–30 (0-18.6)	0-15 (0-9.3)	50.0 (164.0)	3.5 (11.5)	17.2 (56.4)
7*	M_w 9.3 earthquake with 35 m of maximum slip across the majority of the rupture	2–38 (1.2–23.6)	5–22 (3.1-13.7)	35.0 (115.0)	7.8 (25.6)	11.6 (38.0)
8*	M_w 9.3 earthquake with 50 m of maximum slip in the shallow part of the rupture	0–31 (0-19.2)	0–18 (0-11.2)	50.0 (164.0)	9.6 (31.5)	28.0 (91.9)
9*	M_w 9.1 earthquake in the Cascadia subduction zone	45.0 (150.0)	36.0 (120.0)	45.0 (148.0)	8.0 (25.0)	11.0 (35.0)

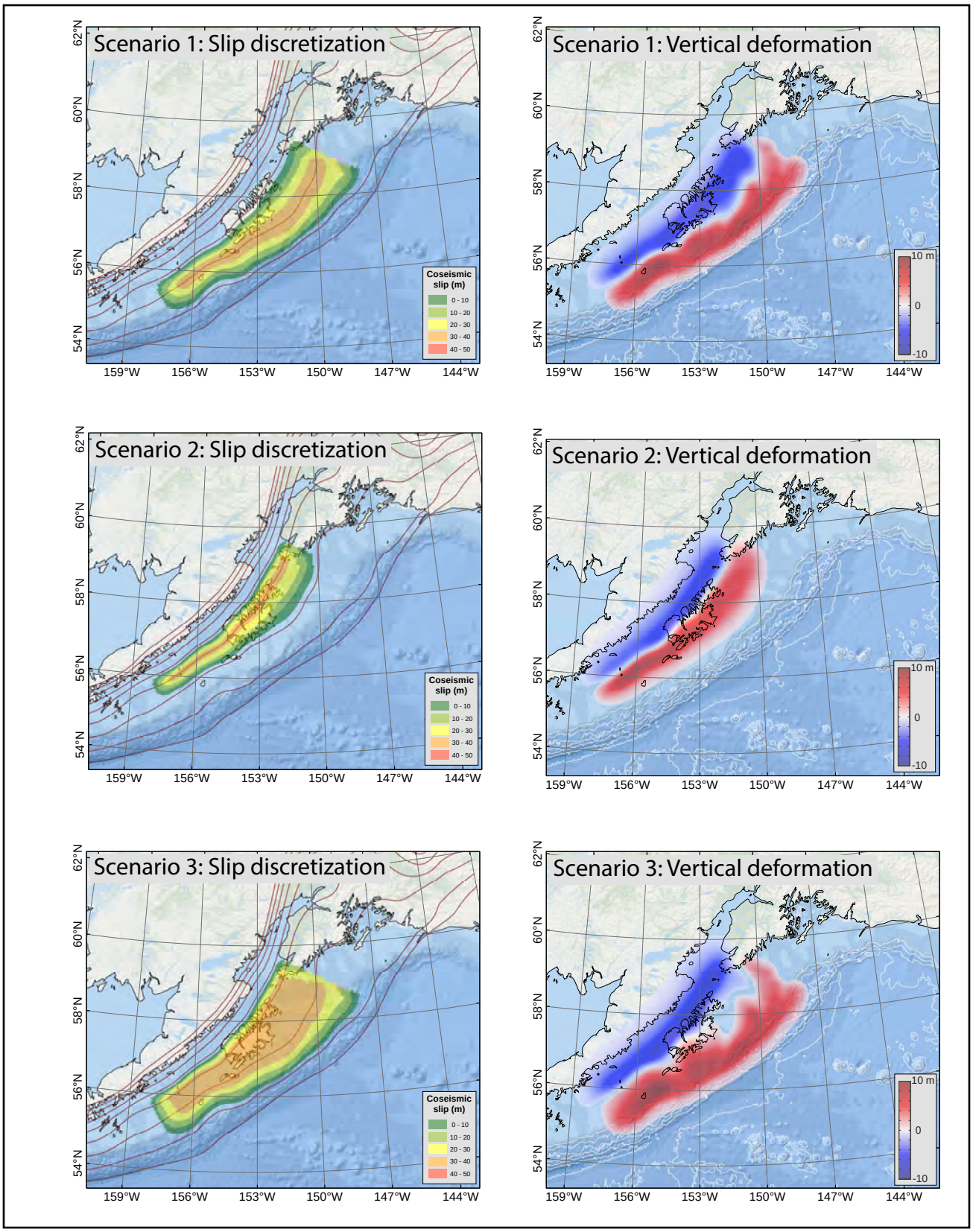

Figure 10A. Estimated slip distribution along the plate interface for scenarios 1–3, and computed vertical ground-surface deformation for scenarios 1–3. Red lines are depth contours of the subduction interface, in kilometers. White lines are bathymetry contours within the depth interval between 1 and 5 km.

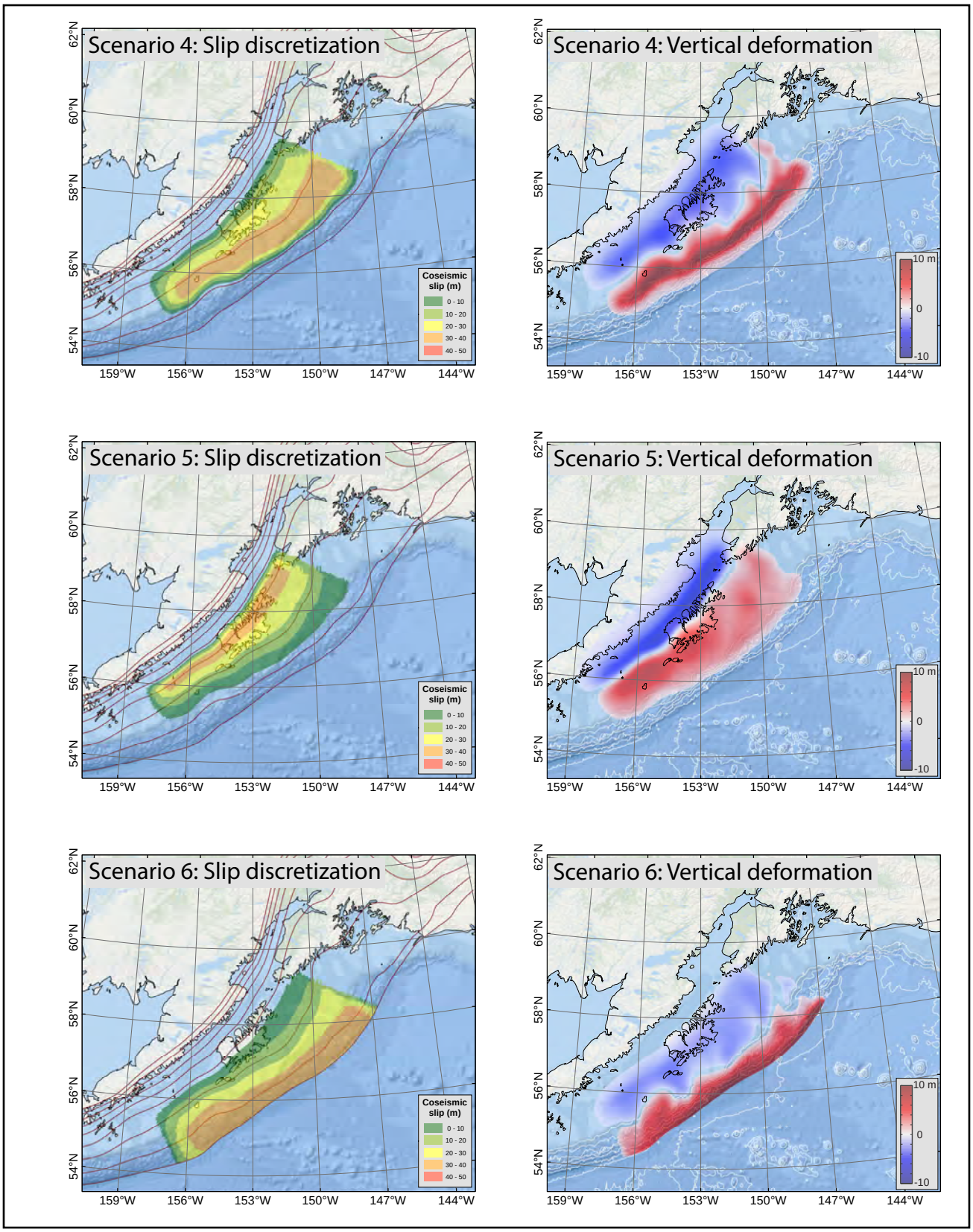

Figure 10B. Estimated slip distribution along the plate interface for scenarios 4–6, and computed vertical ground-surface deformation for scenarios 4–6. Red lines are depth contours of the subduction interface, in kilometers. White lines are bathymetry contours within the depth interval between 1 and 5 km.

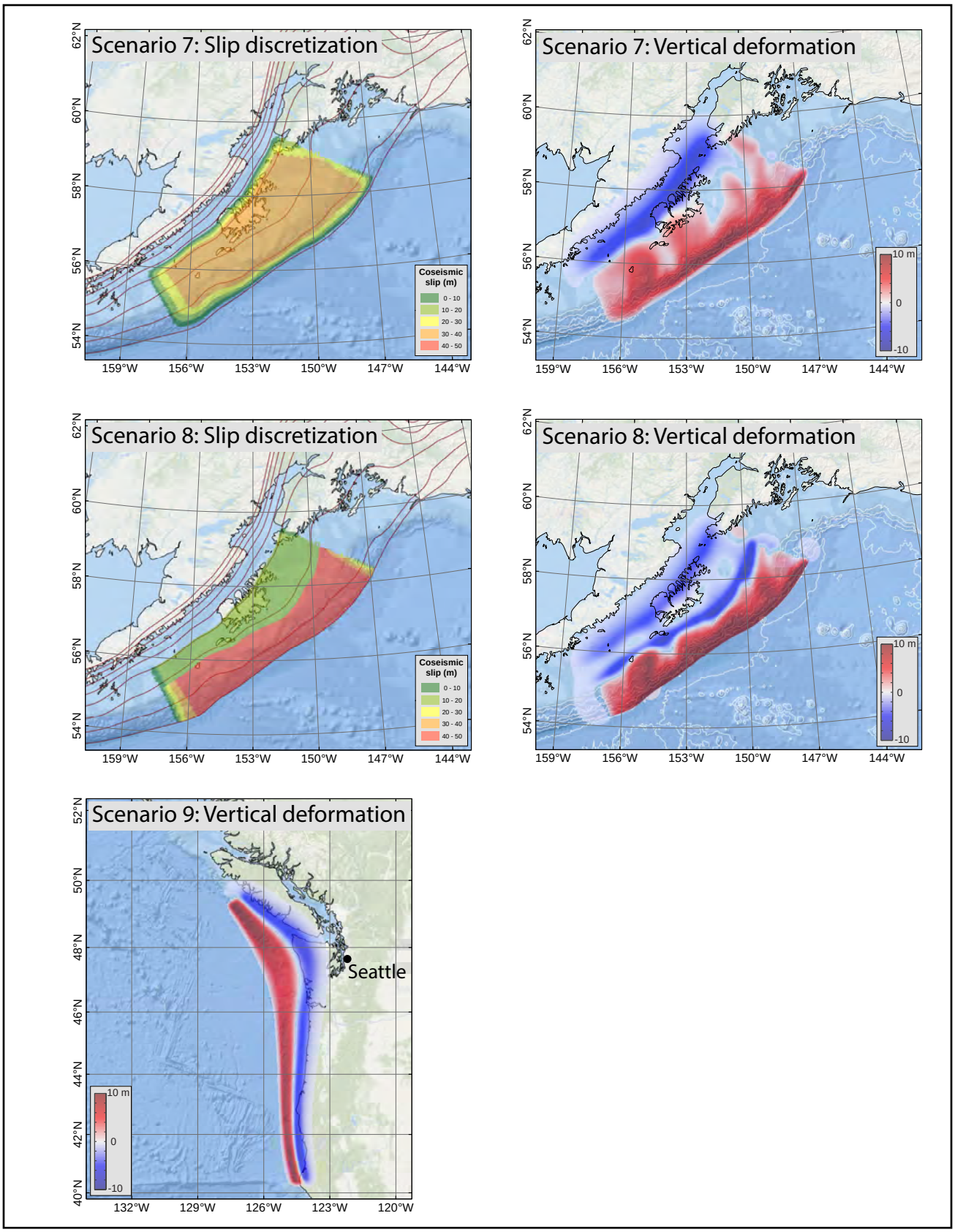

Figure 10C. Estimated slip distribution along the plate interface for scenarios 7–8, and computed vertical ground-surface deformation for scenarios 7–9 (slip distribution is not provided for scenario 9). Red lines are depth contours of the subduction interface, in kilometers. White lines are bathymetry contours within the depth interval between 1 and 5 km.

Blind Rupture Scenarios

Blind rupture scenarios model hypothetical ruptures of the KI segment of the Alaska–Aleutian megathrust. The updip and downdip limits of the rupture are 10 km (6.2 mi) and 40 km (24.8 mi), respectively. The proposed slip distributions and vertical coseismic deformations for scenarios 1–5 are shown in figures 10A and 10B.

Scenario 1: M_W 9.2 near Kodiak Island; 20 km (12.4 mi) depth	The depth of maximum slip corresponds to the depth for sensitivity case C. The slip skewness parameter, q, is set to 0.5 (bell-shaped curve is centered) to model the maximum slip of 35 m (115 ft) at a depth of 20 km (12.4 mi).
Scenario 2: M_W 9.0 near Kodiak Island; 30 km (18.6 mi) depth	The depth of maximum slip corresponds to the depth for sensitivity case D. The slip skewness parameter, q, is set to 0.5 (bell-shaped curve is centered) to model the maximum slip of 35 m (115 ft) at a depth of 30 km (18.6 mi).
Scenario 3: M_W 9.3 near Kodiak Island; 20–30 km (12.4 mi-18.6 mi) depth	The depth of maximum slip corresponds to a combination of sensitivity cases C and D, with the width of the maximum slip area extending from 15 to 35 km (9.3 to 21.7 mi) depth.
Scenario 4: M_W 9.27 near Kodiak Island; 20–30 km (12.4 mi-18.6 mi) depth, q=0.2	The depth of maximum slip corresponds to the depth for sensitivity case C. The slip skewness parameter, q, is set to 0.2 (bell-shaped curve skewed toward the trench) to model the maximum slip of 35 m (115 ft) at a depth of 17 km (10.5 mi), still with significant slip near the trench. The width of the maximum slip extends from 12 to 22 km (6.5 to 13.6 mi) depth.
Scenario 5: M_W 9.18 near Kodiak Island, 20–30 km (12.4 mi-18.6 mi) depth, q=0.7	The depth of maximum slip corresponds to the depth for sensitivity case D. The slip skewness parameter, q, is set to 0.7 (bell-shaped curve skewed toward the deeper part of the rupture) to model the maximum slip of 35 m (115 ft) at a depth of 30 km (18.6 mi). The width of the maximum slip extends from 15 to 25 km (9.3 to 15.5 mi) depth.

Surface-Breaching Rupture Scenarios

Ryan and others (2012), and later Kirby and others (2013), compared the Alaska and Tohoku subduction margins and suggested that a hypothetical rupture in the Alaska–Aleutian subduction zone could propagate to shallow depths as it did in the M_W 9.0 Tohoku earthquake. Shallow fault rupture at the Tohoku margin was manifested as a complex mix of seafloor rupture and blind (concealed) fault-bend folding along the fault length, both of which contributed to significant vertical seafloor disturbance. Multibeam bathymetry in the Kodiak Island

area suggests that the Alaska–Aleutian megathrust has similar, mixed-behavior shallow ruptures. To account for the earthquake deformation front reaching the seafloor, we construct scenarios 6 and 8 with modeled fault slip extending all the way to the zero-depth contour. The updip and downdip limits of the rupture are 0 km (0 mi) and 28 km (17.4 mi), respectively. The proposed slip distribution and vertical coseismic deformations for scenario 6 are shown in figure 10B.

Scenario 6: M_W 9.3 near Kodiak Island; 10 km (6.2 mi) depth of maximum slip, slip extending to the ocean bottom

The region of maximum slip of 50 m (164 ft) extends from the zero-depth contour to the depth of the plate interface of 15 km (9.3 mi), and then slip gradually reduces to about 10 m (33 ft) at the depth of 30 km (18.6 mi).

Recently Butler and others (2014) described a layer of sand discovered in the Makauwahi sinkhole on the island of Kaua'i, Hawai'i. The origin of this layer was attributed to inundation of the sinkhole by a giant paleotsunami following a M_W 9+ earthquake in the eastern Aleutian Islands. Butler (2012) provides an in-depth examination of previous great Aleutian earthquakes and tsunamis impacting Hawai'i. In subsequent research, Butler (2014) considered several hypothetical events with 35 m (114.8 ft) displacement on the megathrust and up to 50 m (164 ft) displacement near the trench. We assume that similar hypothetical events might occur near Kodiak Island and consider two additional scenarios. The proposed slip distribution and vertical coseismic deformations for scenarios 7 and 8 are shown in figure 10C.

Scenario 7: M_W 9.3 earthquake with 35 m of maximum slip across the majority of the rupture

In this scenario we assume 35 m (114.8 ft) of slip for nearly the entire rupture patch between the 5 km (3.1 mi) and 35 km (21.7 mi) depth contours, with slip decreasing both toward the trench and to the deeper parts of the rupture. A similar scenario was proposed in the tsunami modeling study for Kodiak (scenario 8 of Suleimani and others, 2017).

Scenario 8: M_W 9.25 earthquake near Kodiak Island with 50 m (164.0 ft) of maximum slip

In this scenario we assume 20 m (65.6 ft) slip on the plate interface between the 17.9 km (11.1 mi) and 30.8 km (19.1 mi) depth contours, and up to 50 m (164 ft) slip near the trench between 0 km (0 mi) and 17.9 km (11.1 mi) depth. A similar scenario was proposed in the tsunami modeling study for Kodiak (scenario 9 of Suleimani and others, 2017).

Far-field Scenarios

Although a rupture of the Cascadia subduction zone is not a worst-case scenario for the Kodiak Island area, for the sake of community preparedness we also simulate a large hypothetical earthquake along the western seaboard of the U.S.

Scenario 9: Rupture of the Cascadia subduction zone, including the entire megathrust between British Columbia and northern California

This scenario is the same as Scenario 16 in the tsunami modeling studies for King Cove and Cold Bay (Suleimani and others, 2016). The slip distribution model for this scenario is shown in figure 10 of Wang and others (2003). The vertical coseismic deformations for scenario 9 are shown in figure 10C.

MODELING RESULTS

We performed numerical calculations for each of the nine hypothetical earthquake scenarios. Water dynamics are modeled for each grid listed in table 2; the extent of inundation and flow depths are calculated only for the level 4 high-resolution grids. Map sheets 1 and 2 show the maximum composite extent of inundation for all scenarios and the maximum composite flow depths over dry land. The composite values are calculated as follows: for each tsunami scenario, the tsunami flow depth is computed at each grid point and at every time step during the tsunami propagation time the maximum value is kept; then we compute the composite maximum flow depth from all considered scenarios by again choosing the maximum value for each grid point among all scenarios. The same methodology is used to calculate the composite extent of tsunami inundation. The calculated extent of inundation includes coseismic deformation in the communities.

Scenario 3 resulted in the worst inundation at both communities (figs. 11 and 12). We plot the extent of inundation for each community in figures 11 and 12 for five scenarios that are chosen using the following considerations. Scenario 2 is the worst case between scenarios 1 and 2 (cases with the highest slip concentrated in a relatively narrow band at depth). Scenario 3 is the worst case between scenarios 3 and 7 (cases with the highest slip distributed in a wide depth band). Scenario 5 is the worst case between scenarios 4 and 5 (cases with the same total area of slip as in scenario 3, but with more concentrated areas of maximum slip). Scenario 8 is the worst case between scenarios 6 and 8 (surface-breaching rupture scenarios with maximum slip close to the trench). And finally, scenario 9 represents a far-field tsunami event.

Karluk

Karluk is located inside the shallow Karluk Lagoon, which is sheltered by a spit from the waves coming from Shelikof Strait. In Karluk, none of the scenarios inundate the entire community. Scenarios 2, 3, and 5 partially flood Karluk Avenue—greater inundation than scenarios 8 and 9 (fig. 11). Map sheet 1 shows the composite inundation line and flow depths over dry land for Karluk. A part of the community is inside the inundation zone with flow depths reaching 5 m (16.4 ft).

The numerical simulations reveal that the first wave, which is the highest one, could start arriving at Karluk about 20 minutes after the earthquake. As demonstrated by the time series data shown in appendix A (fig. A2), significant wave activity could continue in Karluk for at least 12 hours after the earthquake, and the predicted average time interval between successive waves is 1.5 to 2 hours.

Larsen Bay

In Larsen Bay, scenarios 2, 3, and 5 inundate almost the entire community except for the landing strip and Second Street in the western part of the village. Scenario 8 also floods a significant part of the community, including the area beyond First Street. Scenario 9 results in minimal inundation. Map sheet 2 shows the composite inundation line and flow depths over dry land for Larsen Bay. A major part of the community is inside the inundation zone, with flow depths reaching 8 m (26 ft) near the cannery.

The numerical simulations reveal that the first wave could start arriving at Larsen Bay in less than 30 minutes after the earthquake. The second wave is the largest and reaches maximum height about 2 hours after the earthquake. As demonstrated by the time series shown in appendix B (fig. B2), significant wave activity could continue in Larsen Bay for at least 12 hours after the earthquake, and the predicted average time interval between successive waves is about 1.5 hours.

Time Series

The arrival time of the first wave, the maximum wave amplitude, and the duration of wave action are all important factors that should be considered during evacuation planning. We supplement the inundation maps with time series of the modeled water level and velocity dynamics at selected loca-

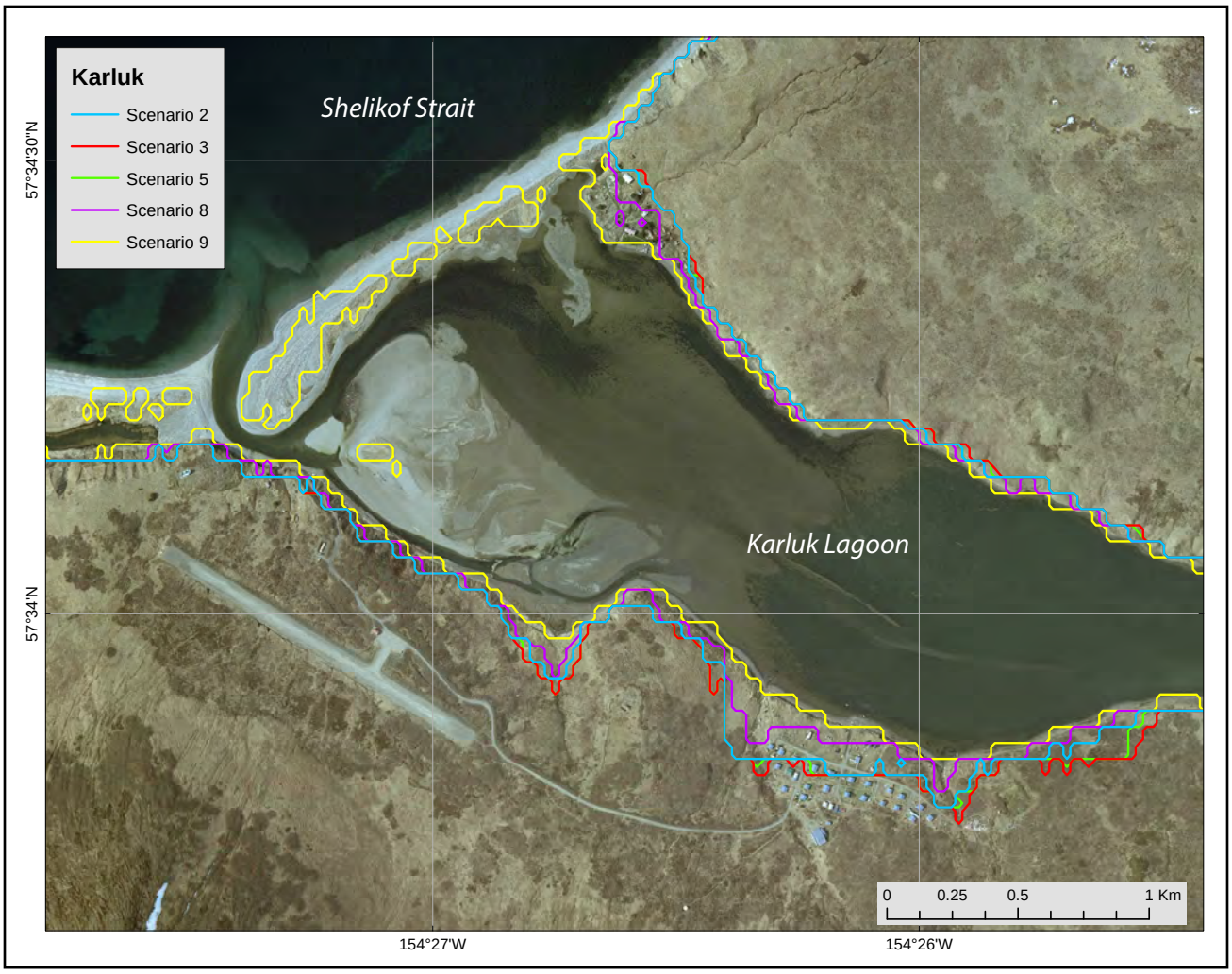

Figure 11. Extents of tsunami inundation at Karluk for selected scenarios.

tions in Karluk and Larsen Bay. Time series plots show that a hypothetical earthquake with a magnitude of 9.0–9.3 could cause devastating waves that inundate significant areas in both communities. Appendices A and B contain plots of sea level and velocity time series for selected scenarios at critical locations. For each location shown by a number in figures A1 and B1, we plot the sea level and water velocity in figures A2 and B2, respectively. Scenarios 2, 3, and 5 are the megathrust scenarios that result in the largest tsunami inundation areas in the communities. Scenario 9 is included as an example of a potential far-field event for Kodiak.

In all time series plots, zero time corresponds to the earthquake event. The pre-earthquake elevation/depth with respect to the MHHW is stated for each location. To show the height of arriving tsunamis for offshore locations, we use a vertical datum (WGS84) with a zero-mark corresponding to the pre-earthquake sea level. The dashed lines show water levels after the tsunami. The velocity magnitude is calculated as water flux divided by water depth, thus the velocity value can have large uncertainties when the water depth is small. In the plots provided, the velocity is computed only where the water depth is greater than 0.3 m (1.0 ft).

SOURCES OF ERRORS AND UNCERTAINTIES

The hydrodynamic model used to calculate propagation and run-up of tectonic tsunamis is a nonlinear, flux-formulated, shallow-water model

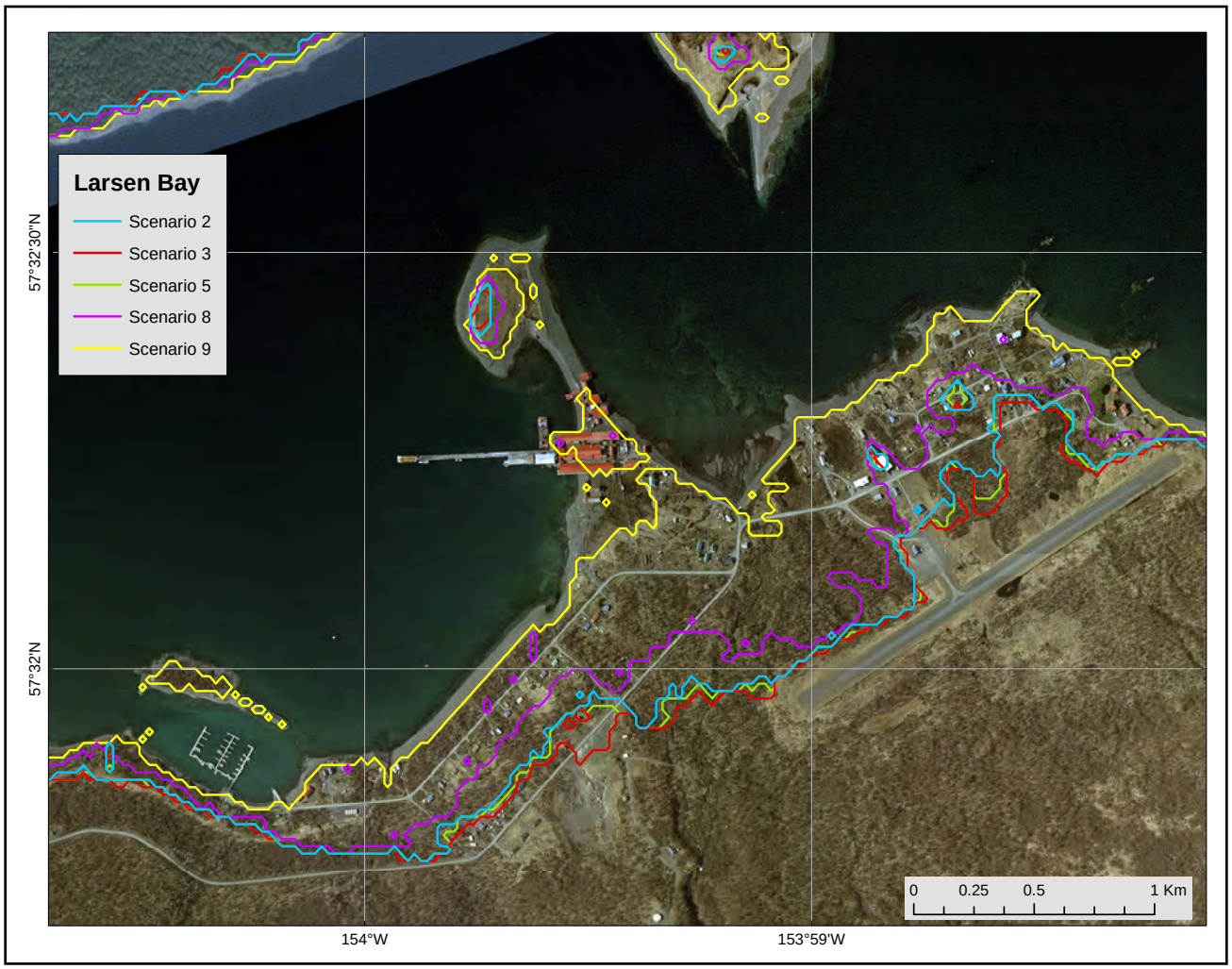

Figure 12. Extents of tsunami inundation at Larsen Bay for selected scenarios.

(Nicolsky, Suleimani, and Hansen, 2011) that passed the verification and validation tests required for numerical codes used to produce tsunami inundation maps (Synolakis and others, 2007; NTHMP, 2012). Most of the errors/uncertainties in the numerical predictions originate from the tsunami sources used in the numerical models. Furthermore, our assessment of potential earthquake scenarios is not exhaustive and only represents a best estimate of the locations and sizes of potential tsunami-generating events. It is possible that other unrecognized earthquake scenarios or slope failures could present hazards to Kodiak communities. However, the scenarios presented are intended to adequately cover the range of potential situations about which the communities should be aware.

The spatial resolution of the grid used to calculate tsunami inundation in Kodiak Island communities is about 16 m (52.5 ft) and satisfies NOAA minimum recommended requirements for computation of tsunami inundation (NTHMP, 2010). This resolution is high enough to describe major relief features; however, small topographic features, buildings, and other facilities cannot be resolved accurately by the existing model. We also note that uncertainty in grid cell elevation/depth propagates into the modeling results and eventually contributes to the horizontal uncertainty in a location of the inundation line. One of the contributors to this uncertainty is the paucity of data in the intertidal zone. However, no established practices exist to directly propagate the DEM uncertainty

into the uncertainty of the inundation line (Hare and others, 2011). In addition to the uncertainty related to the grid cell elevation/depth, uncertainties in the tsunami source (earthquake and splay fault geometry) are the largest source of error in tsunami modeling efforts. The direction of the incoming waves, their amplitudes, and times of arrival are primarily determined by displacements of the ocean surface in the source area. Therefore, the inundation modeling results for local sources are especially sensitive to the fine structure of the tsunami source. The modeling process is highly sensitive to errors when the complexity of the source function is combined with its proximity to the coastal zone.

SUMMARY

We present the results of numerical modeling of earthquake-generated tsunamis for Karluk and Larsen Bay on Kodiak Island, Alaska. The earthquake scenarios considered in this report include a range of magnitudes for ruptures on the Kodiak Island segment of the Alaska–Aleutian megathrust. Hypothetical scenario 3 (M_W 9.3 earthquake near Kodiak Island with maximum slip distributed between the 15 and 35 km [9.3–21.7 mi] depth) results in the "worst case" tsunami-inundation for both communities, while scenarios 2 and 5 produce just slightly smaller inundation areas than scenario 3. The results show that the maximum predicted flow depth in the communities ranges from 5 to 15 m (16.4 to 49.0 ft), and the currents in the surrounding waters can be as strong as 7.2 m/sec (14 knots). Dangerous wave activity is expected to last for at least 12 hours after a major earthquake.

Each of the scenarios considered are geologically reasonable and present potential hazards to the communities. Map sheets 1 and 2, showing the potential extent of inundation and the tsunami flow depths, have been completed using the best information available and are believed to be accurate; however, their preparation required many assumptions. We considered several tsunami scenarios and have provided an estimate of maximum credible tsunami inundation. Actual conditions during a tsunami event may vary from those considered, so the report's accuracy cannot be guaranteed. The limits of inundation shown in map sheets 1 and 2 should only be used as a guideline for emergency planning and response action. Actual inundated areas will depend on specifics of earth deformations, on-land construction, and tide level, and may differ from areas shown on the map. The information on these maps is intended to assist state and local agencies in planning for emergency evacuation and tsunami response actions in the event of a major tsunamigenic earthquake. These results are not intended for land-use regulation or building-code development.

ACKNOWLEDGMENTS

This report was funded by the U.S. Department of Commerce/National Oceanic and Atmospheric Administration (NOAA) through National Tsunami Hazard Mitigation Program Awards NA20NWS4670057 and NA21NWS4670003 to the Alaska Division of Homeland Security & Emergency Management in partnership with the Alaska Earthquake Center and the Alaska Division of Geological & Geophysical Surveys. This does not constitute an endorsement by NOAA. Numerical calculations for this work were supported by High Performance Computing (HPC) resources at the Research Computing Systems unit at the Geophysical Institute, University of Alaska Fairbanks. We thank our reviewers, Corina Allen and one anonymous reviewer, for insightful comments and suggestions that improved the report.

REFERENCES

Briggs, R.W., Engelhart, S.E., Nelson, A.R., Dura, T., Kemp, A.C., Haeussler, P.J., Corbett, D.R., Angster, S.J., and Bradley, L.-A., 2014, Uplift and subsidence reveal a nonpersistent megathrust rupture boundary (Sitkinak Island, Alaska): Geophysical Research Letters, v. 41, no. 7, p. 2,289–2,296. doi.org/10.1002/2014GL059380

Butler, Rhett, 2012, Re-examination of the potential for great earthquakes along the Aleutian island arc with implication for tsunamis in Hawai'i: Seismological Research Letters, v. 83, no. 1, p. 30–39. doi.org/10.1785/gssrl.83.1.29

———2014, Great Aleutian tsunamis: Honolulu, HI, University of Hawai'i at Manoa, Hawai'i Institute of Geophysics & Planetology, Peer-Reviewed Report HIGP-2014-1, 170 p. www.higp.hawaii.edu/reports/2014

Butler, Rhett, Burney, David, and Walsh, David, 2014, Paleo-tsunami evidence on Kaua'i and numerical modeling of a great Aleutian tsunami: Geophysical Research Letters, v. 41, no. 19, p. 6,795–6,802. doi.org/10.1002/2014GL061232

Carignan, K.S., McLean, S.J., Eakins, B.W., Love, M.R., and Sutherland, M., 2013, Digital elevation models of Kodiak, Alaska—Procedures, data sources, and analysis: Boulder, CO, NOAA National Centers for Environmental Information (NCEI). www.ngdc.noaa.gov/dem/report/download/5055

Carver, G.A., and Plafker, George, 2008, Paleoseismicity and neotectonics of the Aleutian subduction zone—An overview, *in* Freymueller, J.T., Haeussler, P.J., Wesson, R.L., and Ekström, G., eds., Active tectonics and seismic potential of Alaska: American Geophysical Union Geophysical Monograph 179, p. 43–63.

Christensen, D.H., and Beck, S.L., 1994, The rupture process and tectonic implications of the Great 1964 Prince William Sound Earthquake: Pure and Applied Geophysics, v. 142, no. 1, p. 29–53. doi.org/10.1007/BF00875967

DeMets, Charles, Gordon, R.C., Argus, D.F., and Stein, Seth, 1990, Current plate motions: Geophysical Journal International, v. 101, no. 2, p. 425–478. doi.org/10.1111/j.1365-246X.1990.tb06579.x

Department of Commerce, Community, and Economic Development (DCCED)/Division of Community and Regional Affairs (DCRA), 2015, Community Database Online, accessed November 22, 2016. www.commerce.alaska.gov/dcra/DCRAExternal

Dunbar, P.K., and Weaver, C.S., 2008, U.S. states and territories national tsunami hazard assessment—Historical record and sources for waves: Technical Report, National Oceanic and Atmospheric Administration and U.S. Geological Survey, 59 p. http://nthmp.tsunami.gov/documents/Tsunami_Assessment_Final.pdf

Eberhart-Phillips, Donna, Christensen, D.H., Brocher, T.M., Hansen, Roger, Ruppert, N.A., Haeussler, P.J., and Abers, G.A., 2006, Imaging the transition from Aleutian subduction to Yakutat collision in central Alaska, with local earthquakes and active source data: Journal of Geophysical Research, v. 111, no. B11, p. 303. http://doi.org/10.1029/2005JB004240

Ferris, Aaron, Abers, G.A., Christensen, D.H., and Veenstra, Elizabeth, 2003, High resolution image of the subducted Pacific(?) plate beneath central Alaska, 50–150 km depth: Earth and Planetary Science Letters, v. 214, no. 3–4, p. 575–588. http://doi.org/10.1016/S0012-821X(03)00403-5

Fine, I.V., Thomson, R.E., Lupton, L.M., and Mundschutz, Stephen, 2018a, Numerical modeling of an Alaska 1964-type tsunami at the Canadian Coast Guard Base in Seal Cove, British Columbia, Canadian Technical Report of Hydrography and Ocean Sciences 321, Ocean Sciences Division, Fisheries and Oceans Canada, Institute of Ocean Sciences, Sidney, BC.

———2018b, Numerical modeling of an Alaska 1964-type tsunami at the Canadian Coast Guard Base in Victoria, British Columbia, Canadian Technical Report of Hydrography and Ocean Sciences 323, Ocean Sciences Division, Fisheries and Oceans Canada, Institute of Ocean Sciences, Sidney, BC.

Freund, L.B., and Barnett, D.M., 1976, A two-dimensional analysis of surface deformation due

to dip-slip faulting: Bulletin of the Seismological Society of America, v. 66, no. 3, p. 667–675.

Freymueller, J.T., Woodard, Hillary, Cohen, S.C., Cross, Ryan, Elliott, Julie, Larsen, C.F., Hreinsdóttir, Sigrún, 2008, Active deformation processes in Alaska, based on 15 years of GPS measurements, *in* Freymueler, J.T., Haeussler, P.J., Wesson, R.L., and Ekström, Göran, eds., Active Tectonics and Seismic Potential of Alaska: Geophysical Monograph Series: Washington, D. C., American Geophysical Union, p. 1–42. doi.org/10.1029/179GM02

Geist, E.L., and Parsons, Tom, 2006, Probabilistic analysis of tsunami hazards: Natural Hazards, v. 37, no. 3, p. 277–314. doi.org/10.1007/s11069-005-4646-z

Gulick, S.P.S., Reece, R.S., Christenson, G.L., Van Avendonk, H.J.A., Worthington, L.L., and Pavlis, T.L., 2013, Seismic images of the Transition fault and the unstable Yakutat–Pacific–North American triple junction: Geology, v. 41, no. 5, p. 571–574. doi.org/10.1130/G33900.1

Hare, Rob, Eakins, B.W., and Amanate, Christopher, 2011, Modelling bathymetric uncertainty: International Hydrographic Review, p. 31–42. journals.lib.unb.ca/index.php/ihr/article/view/20888

Hayes, Gavin, 2018, Slab2-A Comprehensive Subduction Zone Geometry Model: U.S. Geological Survey data release. doi.org/10.5066/F7PV6JNV

Johnson, J.M., Satake, Kenji, Holdahl, S.R., and Sauber, Jeanne, 1996, The 1964 Prince William Sound earthquake—Joint inversion of tsunami waveforms and geodetic data: Journal of Geophysical Research, v. 101, no. B1, p. 523–532. doi.org/10.1029/95JB02806

Kachadoorian, Reuben, and Plafker, George, 1967, Effects of the earthquake of March 27, 1964, on communities of Kodiak Area: U.S. Geological Survey Professional Paper 542-F, 41 p. pubs.usgs.gov/pp/0542f/

Kanamori, Hiroo, 1970, The Alaska earthquake of 1964—Radiation of long-period surface waves and source mechanism: Journal of Geophysical Research, v. 75, no. 26, p. 5,029–5,040. doi.org/10.1029/JB075i026p05029

Kirby, Stephen, Scholl, David, von Huene, Roland, and Wells, Ray, 2013, Alaska earthquake source for the SAFRR tsunami scenario, chapter B, *in* Ross, S.L., and Jones, L.M., eds., The SAFRR (Science Application for Risk Reduction) Tsunami Scenario: U.S. Geological Survey Open-File Report 2013–1170, 40 p. pubs.usgs.gov/of/2013/1170/b/

Kulikov, E.A., Rabinovich, A.B., Fine, I.V., Bornhold, B.D., and Thomson, R.E., 1998, Tsunami generation by landslides at the Pacific coast of North America and the role of tides: Oceanology, v. 38, no. 3, p. 323–328.

Lander, J.F., 1996, Tsunamis affecting Alaska, 1737–1996: Boulder, CO, National Oceanic and Atmospheric Administration, National Geophysical Data Center (NGDC), Key to Geophysical Research Documentation, v. 31, 155 p. ftp.ngdc.noaa.gov/hazards/publications/Kgrd-31.pdf

Larsen, C.F., Motyka, R.J., Freymueller, J.T, Echelmeyer, K.A., and Ivins, E.R., 2004, Rapid uplift of southern Alaska caused by recent ice loss: Geophysical Journal International, v. 158, issue 3, p. 1,118–1,133. doi.org/10.1111/j.1365-246X.2004.02356.x

Lee, H.J., Ryan, Holly, Kayen, R.E., Haeussler, P.J., Dartnell, Peter, and Hampton, M.A., 2006, Varieties of submarine failure morphologies of seismically-induced landslides in Alaskan fjords: Norwegian Journal of Geology (Norsk Geologisk Tidsskrift), v. 86, no. 3, p. 221–230.

Lim, E., Eakins, B.W., and Wigley, R., 2009, Southern Alaska coastal relief model—Procedures, data sources, and analysis: National Geophysical Data Center, NOAA, 25 p. www.ngdc.noaa.gov/mgg/coastal/s_alaska.html

National Centers for Environmental Information (NCEI/WDS), in progress, Global historical tsunami database at NCEI, 2100 BC to present (interactive map): National Centers for Environmental Information, NOAA. doi.org/10.7289/V5PN93H7

National Tsunami Hazard Mapping Program (NTHMP), 2010, Guidelines and best practices

for tsunami inundation modeling for evacuation planning: National Oceanic and Atmospheric Administration (NOAA), NTHMP Mapping & Modeling Subcommittee.

———2012, Proceedings and results of the 2011 NTHMP Model Benchmarking Workshop: Boulder, CO, U.S. Department of Commerce/NOAA/NTHMP, NOAA Special Report, 436 p. nthmp.tsunami.gov

Nicolsky, D.J., Suleimani, E.N., Combellick, R.A., and Hansen, R.A., 2011, Tsunami inundation maps of Whittier and western Passage Canal, Alaska: Alaska Division of Geological & Geophysical Surveys Report of Investigation 2011-7, 65 p. doi.org/10.14509/23244

Nicolsky, D.J., Suleimani, E.N., Freymueller, J.T., and Koehler, R.D., 2015, Tsunami inundation maps of Fox Islands communities, including Dutch Harbor and Akutan, Alaska: Alaska Division of Geological & Geophysical Surveys Report of Investigation 2015-5, 67 p., 2 sheets, scale 1:12,500. doi.org/10.14509/29414

Nicolsky, D.J., Suleimani, E.N., Haeussler, P.J., Ryan, H.F., Koehler, R.D., Combellick, R.A., and Hansen, R.A., 2013, Tsunami inundation maps of Port Valdez, Alaska: Alaska Division of Geological & Geophysical Surveys Report of Investigation 2013-1, 77 p., 1 sheet, scale 1:12,500. doi.org/10.14509/25055

Nicolsky, D.J., Suleimani, E.N., and Hansen, R.A., 2011, Validation and verification of a numerical model for tsunami propagation and runup: Pure and Applied Geophysics, v. 168, no. 6, p. 1,199–1,222. doi.org/10.1007/s00024-010-0231-9

Nicolsky, D.J., Suleimani, E.N., and Koehler, R.D., 2014, Tsunami inundation maps of Cordova and Tatitlek, Alaska: Alaska Division of Geological & Geophysical Surveys Report of Investigation 2014-1, 49 p. doi.org/10.14509/27241

———2016, Tsunami inundation maps for the communities of Chignik and Chignik Lagoon, Alaska: Alaska Division of Geological & Geophysical Surveys Report of Investigation 2016-8, 48 p., 2 sheets, scale 1:12,500. doi.org/10.14509/29675

———2017, Tsunami inundation maps for the city of Sand Point, Alaska: Alaska Division of Geological & Geophysical Surveys Report of Investigation 2017-3, 61 p., 4 sheets, scale 1:15,000. doi.org/10.14509/29706

Nishenko, S.P., 1991, Circum-Pacific seismic potential, 1989–1999: Pure and Applied Geophysics, v. 135, no. 2, p. 169–259. doi.org/10.1007/BF00880240

Nishenko, S.P., and Jacob, K.H., 1990, Seismic potential of the Queen Charlotte–Alaska–Aleutian seismic zone: Journal of Geophysical Research, v. 95, no. B3, p. 2,511–2,532. doi.org/10.1029/JB095iB03p02511

Okada, Yoshimitsu, 1985, Surface deformation due to shear and tensile faults in a half-space: Bulletin of the Seismological Society of America, v. 75, no. 4, p. 1,135–1,154.

Oppenheimer, Michael, Glavovic, B.C., Hinkel, Jochen, van de Wal, Roderik, Magnan, A.K., Abd-Elgawad, Amro, Cai, Rongshuo, Cifuentes-Jara, Miguel, DeConto, R.M., Ghosh, Tuhin, Hay, John, Isla, Federico, Marzeion, Ben, Meyssignac, Benoit, Sebesvari, Zita, 2019, Sea level rise implications for low-lying islands, coasts and communities *in* Pörtner, H.-O., Roberts, D.C., Masson-Delmotte, V., Zhai, P., Tignor, M., Poloczanska, E., Mintenbeck, K., Alegría, A., Nicolai, M., Okem, A., Petzoid, J., Rama, B., Weyer, N.M., eds., IPCC Special Report on the ocean and cryosphere in a changing climate. www.ipcc.ch/site/assets/uploads/sites/3/2019/11/08_SROCC_Ch04_FINAL.pdf

———1969, Tectonics: U.S. Geological Survey Professional Paper 543-I, p. G1–G74.

Plafker, George, and Kachadoorian, Reuben, 1966, Geologic effects of the March 1964 earthquake and associated seismic sea waves on Kodiak and nearby islands, Alaska: U.S. Geological Survey Professional Paper 543–D, 46 p. pubs.usgs.gov/pp/0543d/

Plafker, George, Kachadoorian, Reuben, Eckel, E.B., and Mayo, L.R., 1969, Effects of the earthquake of March 27, 1964, on various communities: U.S. Geological Survey Professional Paper 542-G, 50 p. pubs.usgs.gov/pp/0542g/

Rabinovich, A.B., Thomson, R.E., Krassovski, M.V.,

Stephenson, F.E., and Sinnott, D.C., 2019, Five Great Tsunamis of the 20th Century as Recorded on the Coast of British Columbia: Pure and Applied Geophysics, v. 176, p. 2,887–2,924. doi.org/10.1007/s00024-019-02133-3

Ryan, Holly, von Huene, Roland, Scholl, Dave, and Kirby, Steve, 2012, Tsunami hazards to U.S. coasts from giant earthquakes in Alaska: Eos AGU, v. 93, no. 19, 185 p.

SAFRR Tsunami Modeling Working Group, 2013, Modeling for the SAFRR Tsunami Scenario—Generation, propagation, inundation, and currents in ports and harbors, chap. D, *in* Ross, S.L., and Jones, L.M., eds., The SAFRR (Science Application for Risk Reduction) Tsunami Scenario: U.S. Geological Survey Open-File Report 2013–1170, 136 p. pubs.usgs.gov/of/2013/1170/d/

Shennan, Ian, Barlow, Natasha, Carver, Gary, Davies, Frank, Garrett, Ed, and Hocking, Emma, 2014, Great tsunamigenic earthquakes during the past 1,000 yr on the Alaska megathrust: Geology, v. 42, no. 8, p. 687–690. doi.org/10.1130/G35797.1

Shennan, Ian, Bruhn, Ronald, Barlow, Natasha, Good, Kelly, and Hocking, Emma, 2014, Late Holocene great earthquakes in the eastern part of the Aleutian megathrust: Quaternary Science Reviews, v. 84, p. 86–97. doi.org/10.1016/j.quascirev.2013.11.010

Shirzaei, Manoochehr, Freymueller, J.T., Törnqvist, T.E., 2021, Measuring, modelling, and projecting coastal land subsidence: Nat Rev Earth Environ, no. 2, p. 40–58. doi.org/10.1038/s43017-020-00115-x

Soloviev, S.L., 1990, Tsunamigenic Zones in the Mediterranean Sea: Natural Hazards, v. 3, p. 183–202.

Suito, Hisashi, and Freymueller, J.T., 2009, A viscoelastic and afterslip postseismic deformation model for the 1964 Alaska earthquake: Journal of Geophysical Research, v. 114, no. B11, p. 404–426. doi.org/10.1029/ 2008JB005954

Suleimani, E.N., Combellick, R.A., Marriott, D., Hansen, R.A., Venturato, A.J., and Newman, J.C., 2005, Tsunami hazard maps of the Homer and Seldovia areas, Alaska: Alaska Division of Geological & Geophysical Surveys Report of Investigation 2005-2, 28 p., 2 sheets, scale 1:12,500. doi.org/10.14509/14474

Suleimani, E.N., and Freymueller, J.T., 2020, Near-field modeling of the 1964 Alaska tsunami: The role of splay faults and horizontal displacements: Journal of Geophysical Research: Solid Earth, v. 125. doi.org/10.1029/2020JB019620

Suleimani, E.N., Nicolsky, D.J., and Koehler, R.D., 2013, Tsunami inundation maps of Sitka, Alaska: Alaska Division of Geological & Geophysical Surveys Report of Investigation 2013-3, 76 p., 1 sheet, scale 1:250,000. doi.org/10.14509/26671

———2015, Tsunami inundation maps of Elfin Cove, Gustavus, and Hoonah, Alaska: Alaska Division of Geological & Geophysical Surveys Report of Investigation 2015-1, 79 p. doi.org/10.14509/29404

———2017, Updated tsunami inundation maps of the Kodiak area, Alaska: Alaska Division of Geological & Geophysical Surveys Report of Investigation 2017-8, 38 p., 10 sheets. doi.org/10.14509/29740

Suleimani, E.N., Nicolsky, D.J., Koehler, R.D., Freymueller, J.T., and Macpherson, A.E., 2016, Tsunami inundation maps for King Cove and Cold Bay communities, Alaska: Alaska Division of Geological & Geophysical Surveys Report of Investigation 2016-1, 73 p., 2 sheets, scale 1:12,500. doi.org/10.14509/29565

Suleimani, E.N., Nicolsky, D.J., West, D.A., Combellick, R.A., and Hansen, R.A., 2010, Tsunami inundation maps of Seward and northern Resurrection Bay, Alaska: Alaska Division of Geological & Geophysical Surveys Report of Investigation 2010-1, 47 p., 3 sheets, scale 1:12,500. doi.org/10.14509/21001

Synolakis, C.E., Bernard, E.N., Titov, V.V., Kânoğlu, Utku, and González, F.I., 2007, Standards, criteria, and procedures for NOAA evaluation of tsunami numerical models: Seattle, National Oceanic and Atmospheric Administration (NOAA)/Pacific Marine Environmental Laboratory (PMEL), Technical Memorandum OAR PMEL-135, 55 p. www.pmel.noaa.gov/pubs/PDF/syno3053/syno3053.pdf

Wang, Kelin, Sun, Tianhaozhe, Brown, Lonn, Hino, Ryota,Tomita, Fumiaki, Kido, Moyoyuki, Iinuma, Takeshi, Kodaira, Shuichi, and Fujiwara,Toshiya, 2018, Learning from crustal deformation associated with the M9 2011 Tohoku-oki earthquake: Geosphere, v. 14, no. 2, p. 552–571. doi.org/10.1130/GES01531.1

Wang, Kelin, Wells, R.E., Mazzotti, Stephane, Hyndman, R.D., and Sagiya, Takeshi, 2003, A revised dislocation model of interseismic deformation of the Cascadia subduction zone: Journal of Geophysical Research, v. 108, no. B1, p. 2,026–2,038. doi.org/10.1029/2001JB001227

Worthington, L.L., Gulick, S.P.S., and Pavlis, T.L., 2010, Coupled stratigraphic and structural evolution of a glaciated orogenic wedge, offshore St. Elias orogen, Alaska: Tectonics, v. 29, no. 6, TC6013. doi.org/10.1029/2010TC002723

Worthington, L.L., Van Avendonk, H.J.A., Gulick, S.P.S., Christeson, G.L., and Pavlis, T.L., 2012, Crustal structure of the Yakutat terrane and the evolution of subduction and collision in southern Alaska: Journal of Geophysical Research, v. 117, no. B1, B01102. doi.org/10.1029/2011JB008493

Zweck, Chris, Freymueller, J.T., and Cohen, S.C., 2002, Three-dimensional elastic dislocation modeling of the postseismic response to the 1964 Alaska earthquake: Journal of Geophysical Research, v. 107, no. B4. doi.org/10.1029/2001JB000409

APPENDIX A

Figure A1. Locations of time series points in and around Karluk. The longitude and latitude locations of the time series points are listed in table A1.

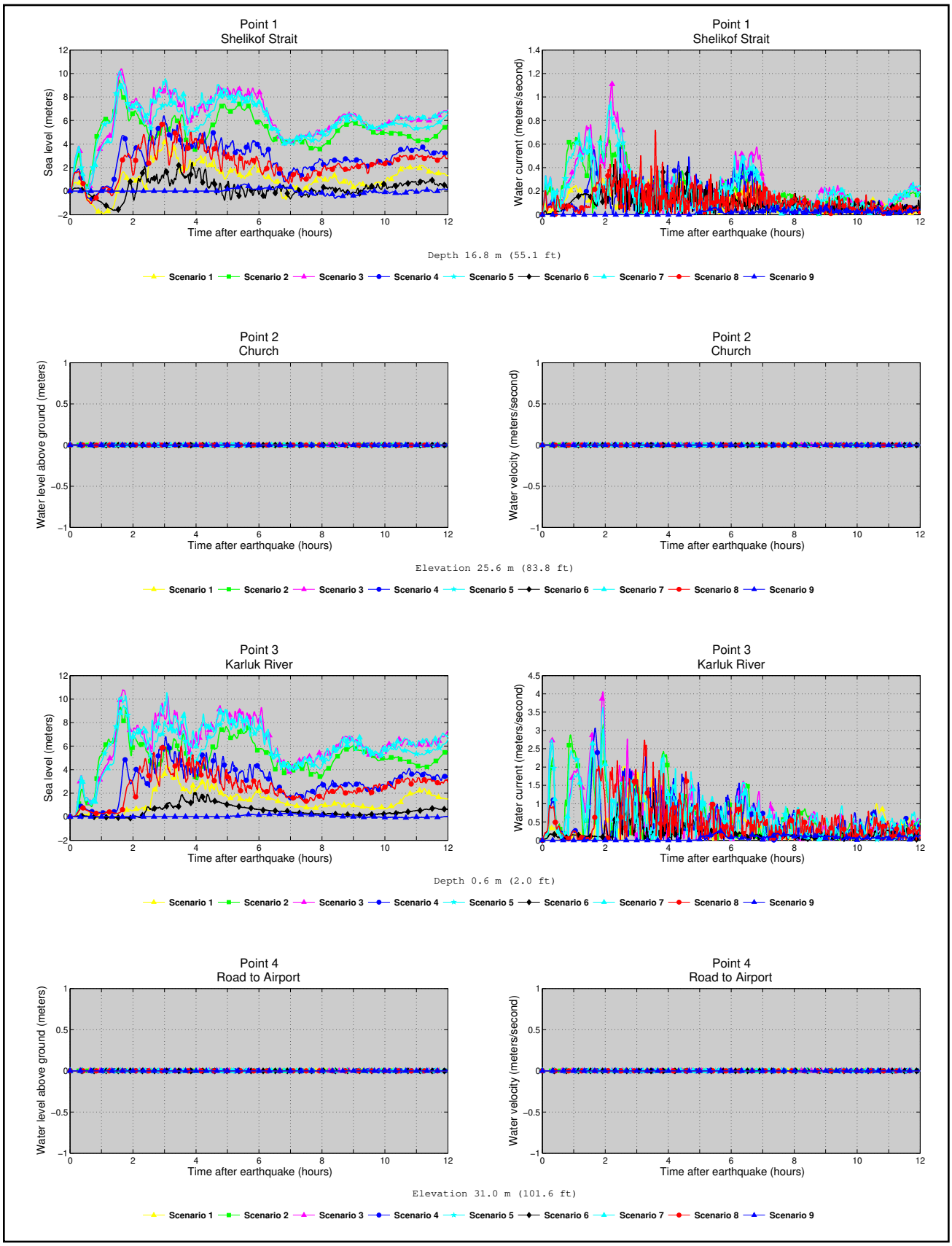

Figure A2. Time series of water level (left column) and velocity (right column) for selected scenarios at locations shown in figure A1. Elevations of onshore locations and ocean depth at offshore locations are given based on the pre-earthquake MHHW datum.

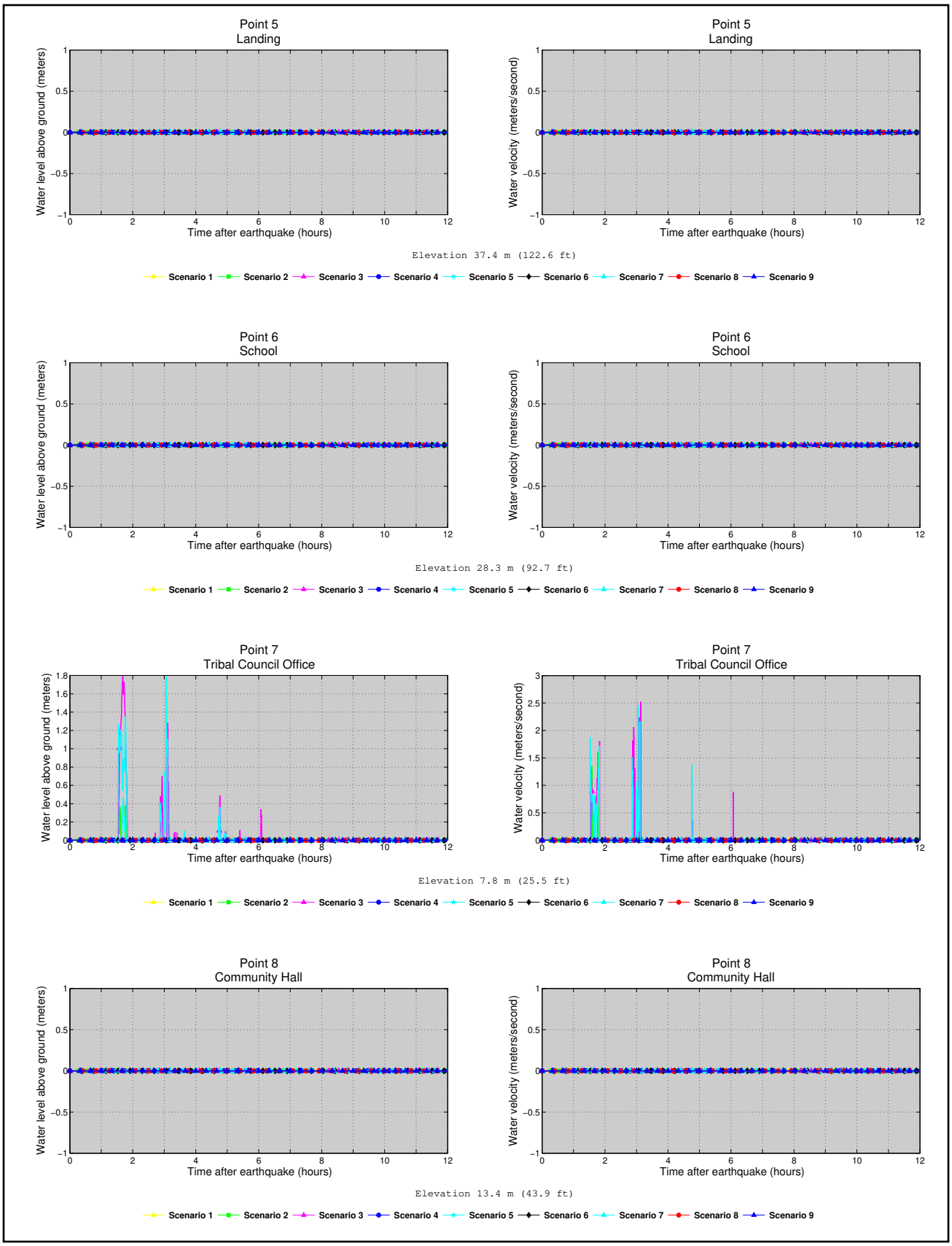

Figure A2, continued. Time series of water level (left column) and velocity (right column) for selected scenarios at locations shown in figure A1. Elevations of onshore locations and ocean depth at offshore locations are given based on the pre-earthquake MHHW datum.

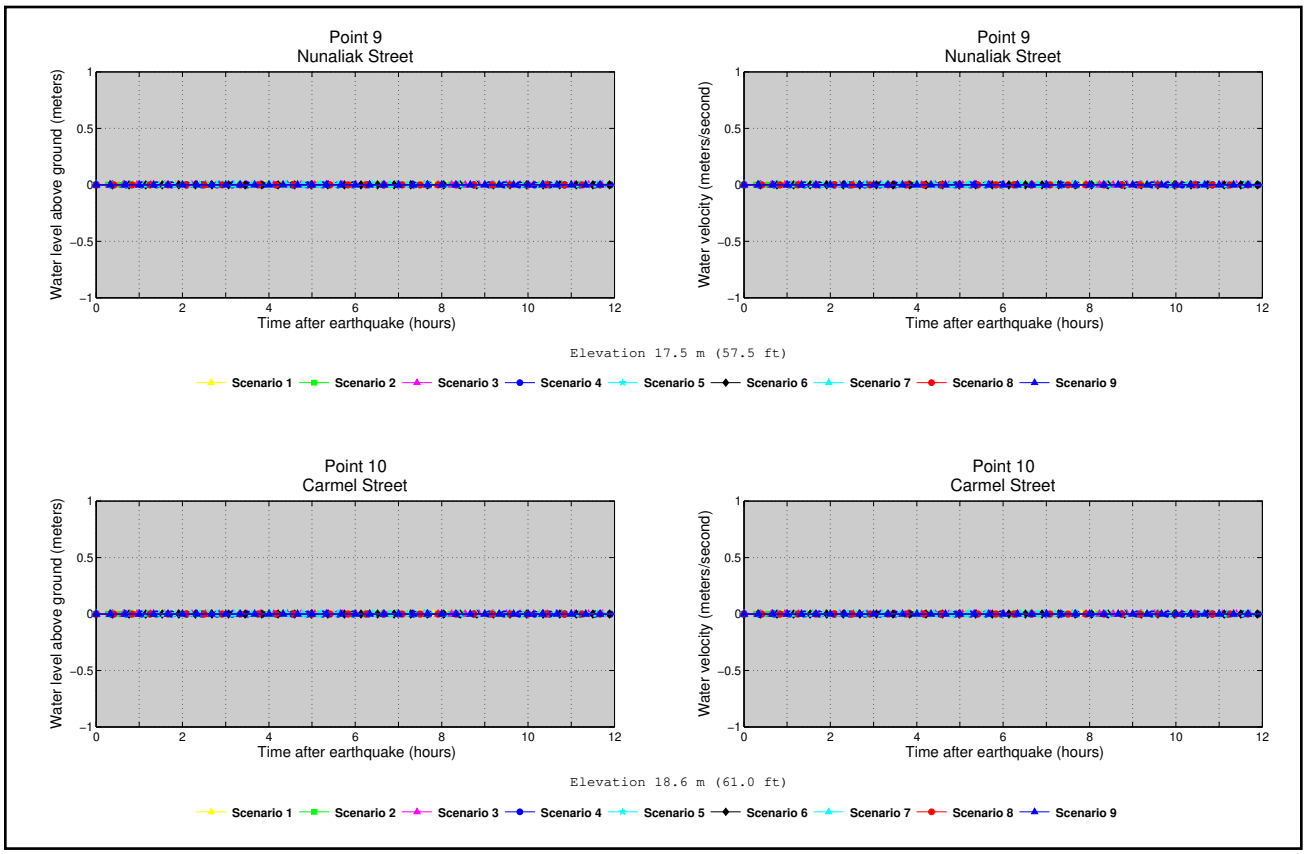

Figure A2, continued. Time series of water level (left column) and velocity (right column) for selected scenarios at locations shown in figure A1. Elevations of onshore locations and ocean depth at offshore locations are given based on the pre-earthquake MHHW datum.

Table A1. Maximum water levels for all tsunami scenarios at time series points in Karluk. The maximum water depth above ground is provided for onshore (S) locations, whereas the maximum water level above the pre-earthquake MHHW is provided for offshore (O) locations.

#	Label	S / O	Longitude (°W)	Latitude (°N)	Minimum elevation/ depth (meters)	Maximum water depth above ground/sea level (meters)								
						Scenario								
						1	2	3	4	5	6	7	8	9
1	Shelikof Strait	O	-154.463056	57.575278	16.8	4.2	9.4	10.4	6.4	10.2	2.4	9.5	5.9	0.6
2	Church	S	-154.458333	57.569167	20.5	0	0	0	0	0	0	0	0	0
3	Karluk River	O	-154.433889	57.566944	0.6	4.4	9.3	10.8	6.8	10.3	2.1	10.5	6.1	0.3
4	Road to Airport	S	-154.453333	57.56750	25.9	0	0	0	0	0	0	0	0	0
5	Landing	S	-154.452222	57.565556	32.3	0	0	0	0	0	0	0	0	0
6	School	S	-154.436944	57.56250	23.2	0	0	0	0	0	0	0	0	0
7	Tribal Council Office	S	-154.435556	57.563889	2.7	0	0.4	1.8	0	1.3	0	1.8	0	0
8	Community Hall	S	-154.437778	57.563611	8.3	0	0	0	0	0	0	0	0	0
9	Nunaliak Street	S	-154.436111	57.563333	12.4	0	0	0	0	0	0	0	0	0
10	Carmel Street	S	-154.433611	57.563056	13.5	0	0	0	0	0	0	0	0	0

Table A2. Maximum water velocities for all tsunami scenarios at time series points in Karluk. The maximum water depth above ground is provided for onshore locations (S), whereas the maximum water level above the pre-earthquake MHHW is provided for offshore (O) locations.

#	Label	S / O	Longitude (°W)	Latitude (°N)	Minimum elevation/ depth (meters)	Maximum water velocity (meters/second)								
						Scenario								
						1	2	3	4	5	6	7	8	9
1	Shelikof Strait	O	-154.463056	57.575278	16.8	0.4	0.7	1.1	0.6	1.0	0.4	0.7	0.7	0.1
2	Church	S	-154.458333	57.569167	20.5	0	0	0	0	0	0	0	0	0
3	Karluk River	O	-154.433889	57.566944	0.6	2.0	3.2	4.1	3.1	3.6	1.4	3.0	2.7	0.3
4	Road to Airport	S	-154.453333	57.56750	25.9	0	0	0	0	0	0	0	0	0
5	Landing	S	-154.452222	57.565556	32.3	0	0	0	0	0	0	0	0	0
6	School	S	-154.436944	57.56250	23.2	0	0	0	0	0	0	0	0	0
7	Tribal Council Office	S	-154.435556	57.563889	2.7	0	1.6	2.5	0	1.9	0	2.5	0	0
8	Community Hall	S	-154.437778	57.563611	8.3	0	0	0	0	0	0	0	0	0
9	Nunaliak Street	S	-154.436111	57.563333	12.4	0	0	0	0	0	0	0	0	0
10	Carmel Street	S	-154.433611	57.563056	13.5	0	0	0	0	0	0	0	0	0

APPENDIX B

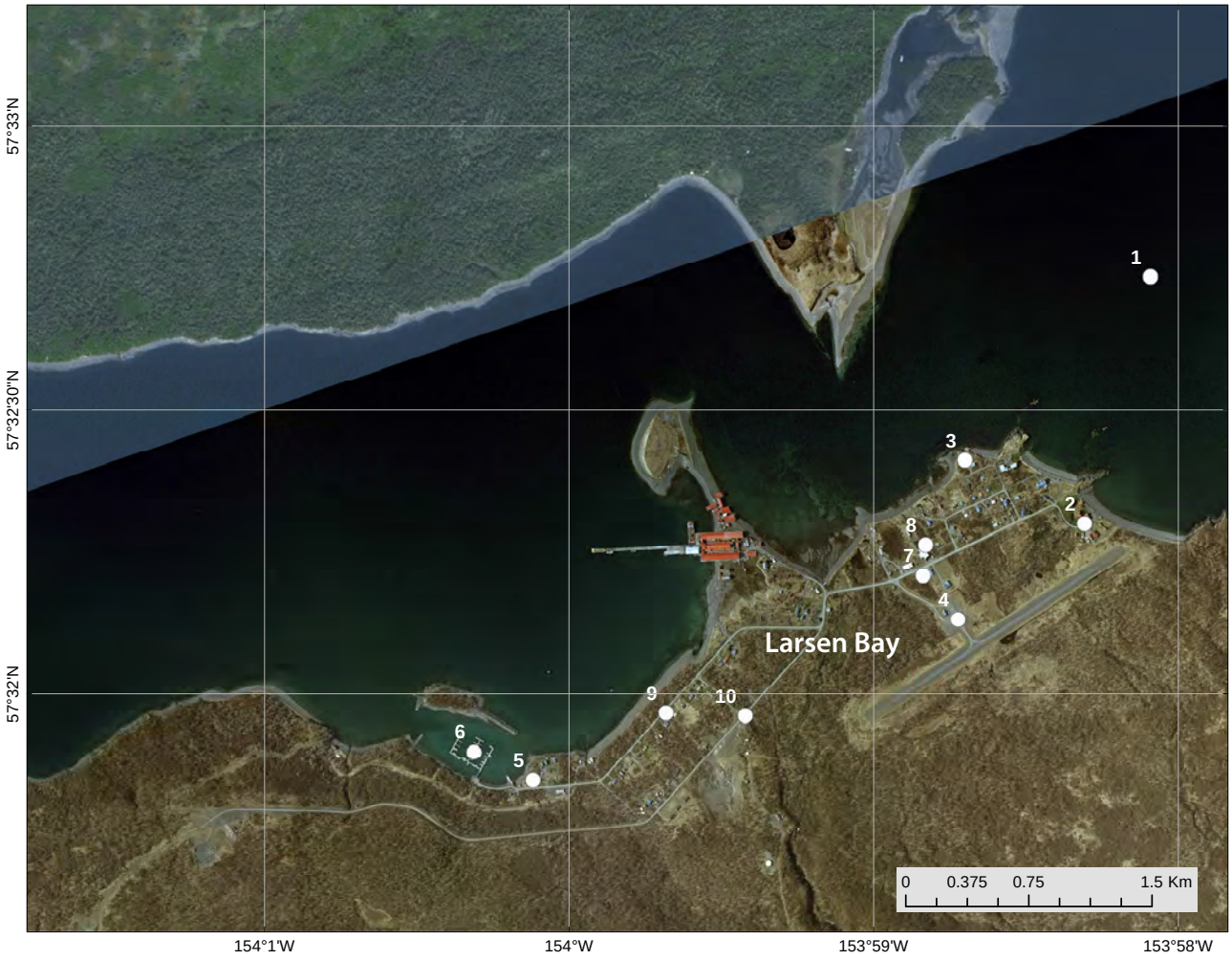

Figure B1. Locations of time series points in and around Larsen Bay. The longitude and latitude locations of the time series points are listed in table B1.

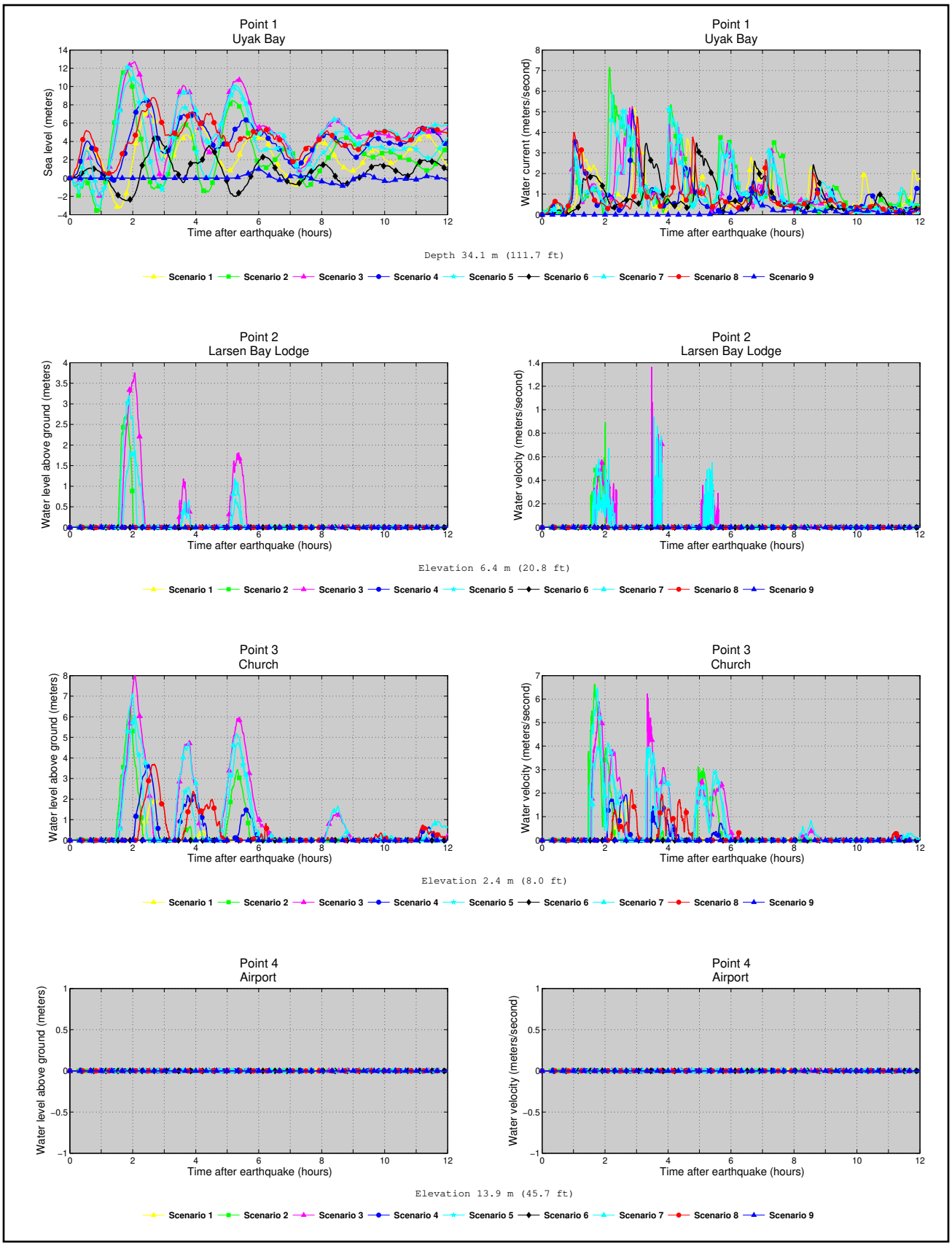

Figure B2. Time series of water level (left column) and velocity (right column) for selected scenarios at locations shown in figure B1. Elevations of onshore locations and ocean depth at offshore locations are given based on the pre-earthquake MHHW datum.

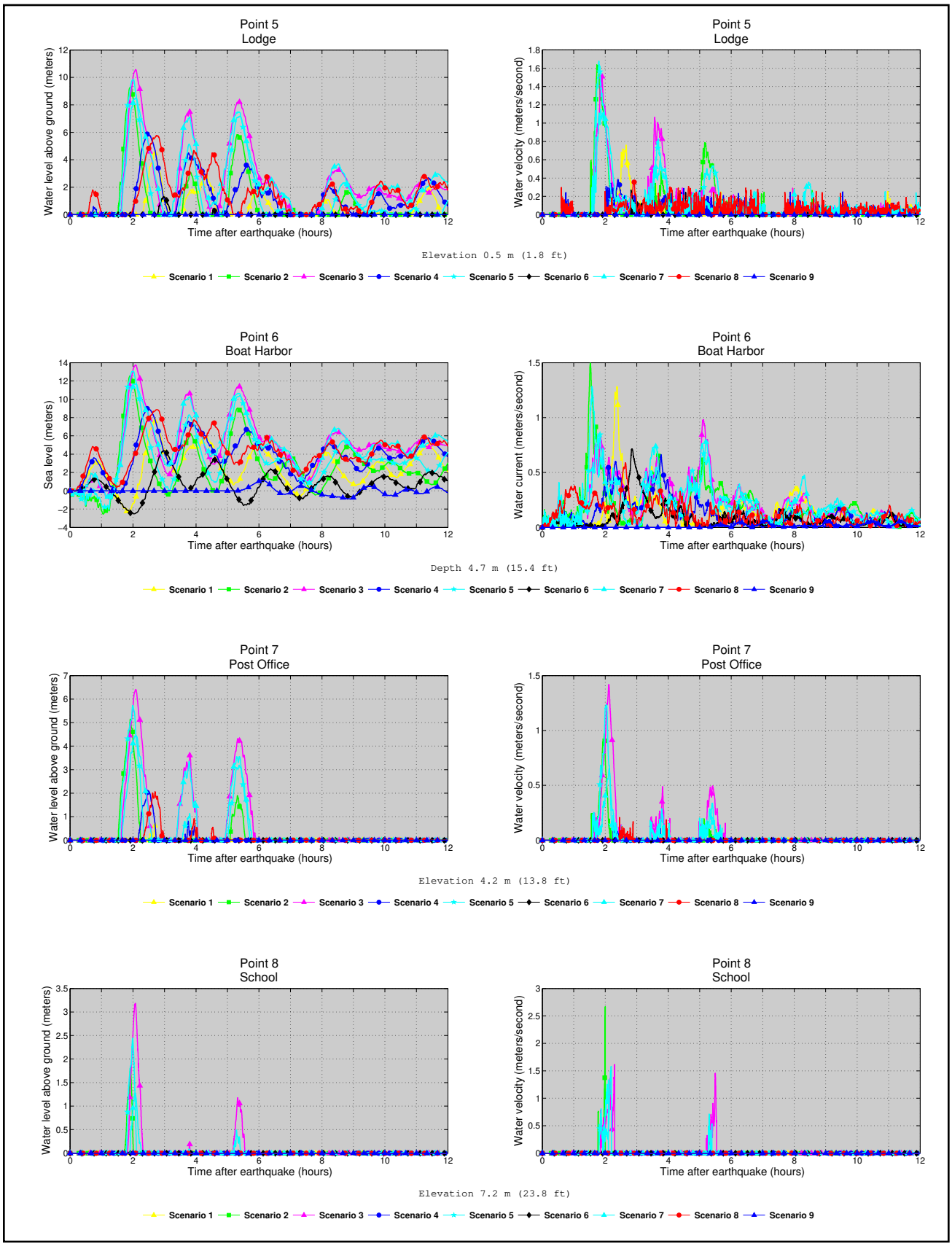

Figure B2, continued. Time series of water level (left column) and velocity (right column) for selected scenarios at locations shown in figure B1. Elevations of onshore locations and ocean depth at offshore locations are given based on the pre-earthquake MHHW datum.

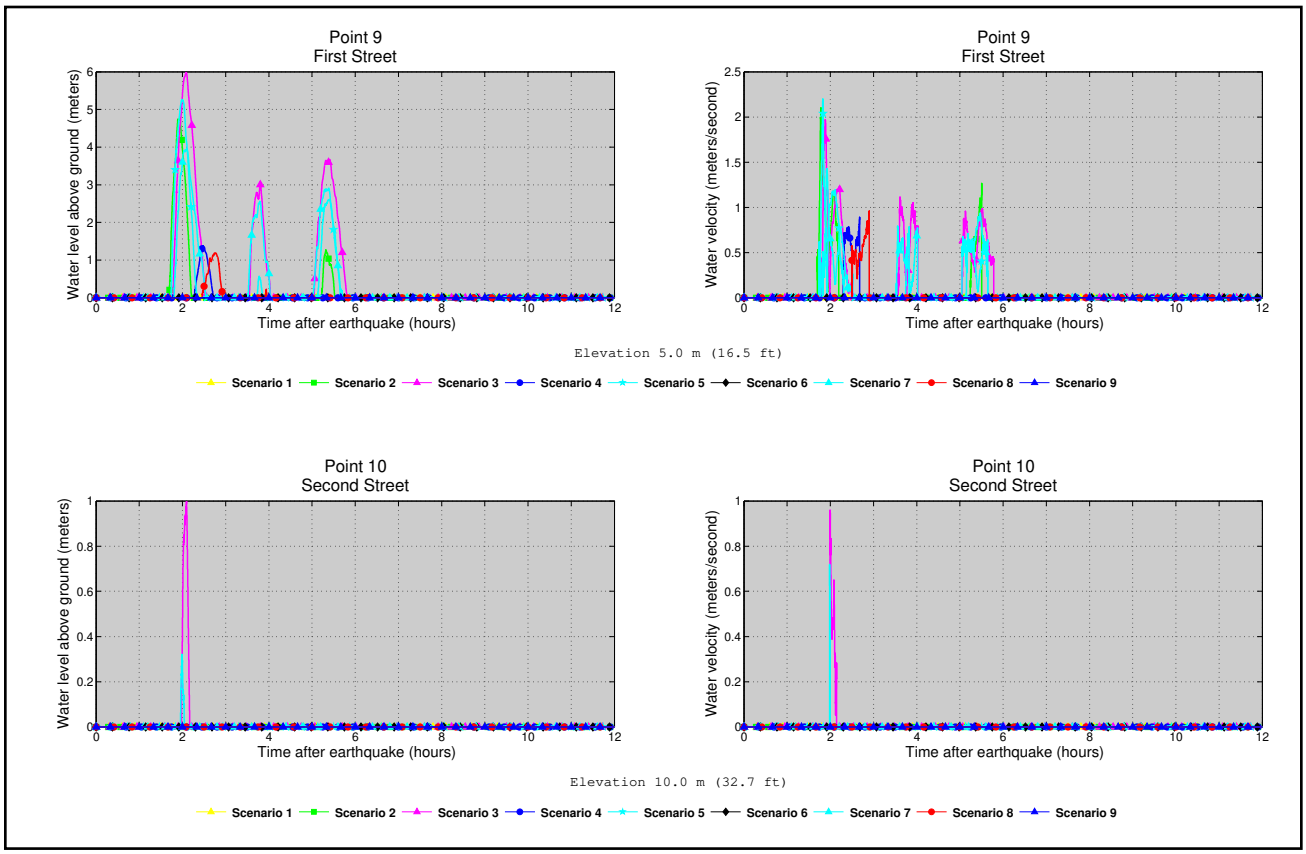

Figure B2, continued. Time series of water level (left column) and velocity (right column) for selected scenarios at locations shown in figure B1. Elevations of onshore locations and ocean depth at offshore locations are given based on the pre-earthquake MHHW datum.

Table B1. Maximum water levels for all tsunami scenarios at time series points in Larsen Bay. The maximum water depth above ground is provided for onshore (S) locations, whereas the maximum water level above the pre-earthquake MHHW is provided for offshore (O) locations.

#	Label	S / O	Longitude (°W)	Latitude (°N)	Minimum elevation/ depth (meters)	Maximum water depth above ground/sea level (meters)								
						Scenario								
						1	2	3	4	5	6	7	8	9
1	Uyak Bay	O	-153.968139	57.545556	34.1	7.3	11.8	12.7	8.6	12.3	4.6	10.8	8.8	1.0
2	Larsen Bay Lodge	S	-153.971750	57.538306	3.8	0	2.8	3.7	0	3.2	0	1.9	0	0
3	Church	S	-153.978278	57.540167	-0.2	1.9	6.5	8.0	3.7	7.1	0	6.1	3.7	0
4	Airport	S	-153.978667	57.53550	11.4	0	0	0	0	0	0	0	0	0
5	Lodge	S	-154.001917	57.530778	-2.1	4.6	9.3	10.6	5.9	9.8	1.3	8.5	5.8	0
6	Boat Harbor	O	-154.005139	57.531611	4.7	7.6	12.6	13.8	9.0	13.1	4.4	11.7	8.9	1.1
7	Post Office	S	-153.980583	57.536778	1.6	0.6	5.2	6.4	2.1	5.7	0	4.4	2.1	0
8	School	S	-153.980444	57.537694	4.6	0	1.8	3.2	0	2.4	0	1.3	0	0
9	First Street	S	-153.994639	57.532750	2.4	0.1	4.7	6.0	1.4	5.3	0	3.9	1.2	0
10	Second Street	S	-153.990306	57.532667	7.4	0	0	1.0	0	0.3	0	0	0	0

Table B2. Maximum water velocities for all tsunami scenarios at time series points in Larsen Bay. The maximum water depth above ground is provided for onshore (S) locations, whereas the maximum water level above the pre-earthquake MHHW is provided for offshore (O) locations.

#	Label	S / O	Longitude (°W)	Latitude (°N)	Minimum elevation/ depth (meters)	Maximum water velocity (meters/second)								
						Scenario								
						1	2	3	4	5	6	7	8	9
1	Uyak Bay	O	-153.968139	57.545556	34.1	5.2	7.2	5.3	5.1	5.9	3.5	4.3	4.8	1.1
2	Larsen Bay Lodge	S	-153.971750	57.538306	3.8	0	0.9	1.4	0	0.7	0	0.9	0	0
3	Church	S	-153.978278	57.540167	-0.2	1.6	6.6	6.2	1.9	6.5	0	4.0	2.2	0
4	Airport	S	-153.978667	57.53550	11.4	0	0	0	0	0	0	0	0	0
5	Lodge	S	-154.001917	57.530778	-2.1	0.8	1.6	1.5	0.4	1.7	0.3	1.2	0.4	0
6	Boat Harbor	O	-154.005139	57.531611	4.7	1.3	1.5	1.0	0.7	1.3	0.7	0.8	0.6	0.1
7	Post Office	S	-153.980583	57.536778	1.6	0	1.0	1.4	0.2	1.2	0	0.7	0.2	0
8	School	S	-153.980444	57.537694	4.6	0	2.7	1.6	0	1.3	0	1.6	0	0
9	First Street	S	-153.994639	57.532750	2.4	0	2.1	2.0	0.9	2.2	0	1.4	1.0	0
10	Second Street	S	-153.990306	57.532667	7.4	0	0	1.0	0	0.7	0	0	0	0